

1 **Characterization of N distribution in different organs of winter wheat**

2 **using UAV-based remote sensing**

3 **Falv Wang¹, Wei Li¹, Yi Liu¹, Weilong Qin¹, Longfei Ma², Yinghua Zhang^{1,3}, Zhencai Sun^{1,3*},**
4 **Zhimin Wang^{1,3}, Fei Li⁴, Kang Yu^{5,1*}**

5 1 College of Agronomy and Biotechnology, China Agricultural University, Beijing, 100193, China

6 2 School of Remote Sensing and Information Engineering, Wuhan University, 430079, China

7 3 Engineering Technology Research Center for Agriculture in Low Plain Areas, Heibei Province, China

8 4 College of Grassland, Resources and Environment, Inner Mongolia Agricultural University, Hohhot, 010011,
9 China

10 5 Precision Agriculture Lab, School of Life Sciences, Technical University of Munich, Freising, 85354, Germany

11 * Correspondence: kang.yu@tum.de

12 **Abstract**

13 Although unmanned aerial vehicle (UAV) remote sensing is widely used for high-throughput crop
14 monitoring, few attempts have been made to assess nitrogen content (NC) at the organ level and its
15 impact on nitrogen use efficiency (NUE). Also, little is known about the performance of UAV-based
16 image texture features in crop nitrogen and NUE monitoring. In this study, eight flying missions
17 were carried out throughout different stages of winter wheat (from the jointing stage to the stage 25
18 days after flowering) to acquire multispectral images. Forty-three multispectral vegetation indices
19 (VIs) and forty texture features (TFs) were calculated from images and fed into the partial least
20 squares regression (PLSR) and random forest (RF) regression models for predicting nitrogen-related
21 indicators. Our main purposes were to (1) evaluate the potential of UAV-based images to predict
22 NC in different organs of winter wheat and nitrogen agronomic efficiency (NAE); (2) compare the
23 performances of VIs, TFs and the combination of them for nitrogen monitoring. The results showed
24 that the correlation between different features (VIs and TFs) and NC in different organs varied
25 between the vegetative and reproductive phases. Most of VIs were found to be positively correlated
26 with NC, while most of the TFs were negatively correlated with NC. PLSR latent variables extracted
27 from VIs and TFs explained 80% of the variations in NAE. However, no significant differences
28 were found between VIs and TFs in their performance in predicting NC in different organs. This
29 study demonstrated the promise of applying UAV-based imaging to estimate NC and NAE in
30 different organs of winter wheat.

31 **Keywords:** unmanned aerial vehicle; organs; nitrogen content monitoring; nitrogen agronomic
32 efficient; vegetation indices; texture features; vegetative and reproductive growth phases

33 **1 Introduction**

34 Higher requirements for crop yield and quality are needed in modern society. Nitrogen (N), as
35 a vital macronutrient, has always been regarded as a key factor in improving crop yield and quality
36 (Wang et al., 2016). In order to ensure high yield, excessive use of N fertilizers in agricultural
37 production have been reported in the North China Plain (NCP) (Cui et al., 2008). Excessive use of
38 N fertilizer causes environmental problems such as soil acidification and water pollution (Ju et al.,
39 2009; Schroder et al., 2011). However, insufficient and inefficient (e.g., wrong time) N fertilizer
40 applications affect the photosynthesis of crops, resulting in reduced crop yield and poor quality
41 (Chlingaryan et al., 2018; Sinclair et al., 2019). Efficient N management for improved N use
42 efficiency (NUE) is critical not only for grain yield and quality but also for environment
43 conservation. Thus, continuous monitoring of crop N status is necessary for the planning of N
44 fertilization measures in the vegetative growth phase and for providing valuable information
45 forecasting yield quality in the reproductive phase (Hank et al., 2019).

46 Traditional methods for crop N status monitoring based on field destructive sampling and
47 chemical analysis such as the Kjeldahl technique has the disadvantages of being time-consuming,
48 labor-intensive and costly, limiting the progress in accurate and continuous assessment of crop N
49 status in field (Yao et al., 2015; Onojeghuo et al., 2018). A portable chlorophyll meter was first used
50 for the diagnosis of the leaf N content of rice, and achieved great performance (T. et al., 1986).
51 Subsequently, many studies using portable chlorophyll meters such as SPAD-502 for the monitoring
52 of crop NC have been reported (Errecart et al., 2012; Yuan et al., 2016; Kitonyo et al., 2018). Besides,
53 other handheld crop sensors like GreenSeeker, Crop Circle multispectral active canopy sensors have
54 been developed and applied in the diagnosing of crop N status (Li et al., 2008; Stroppiana et al.,
55 2009; Cao et al., 2013). However, most proximal sensing tools face the challenge of limited
56 throughput. In recent years, the newly emerged UAV remote sensing technology has allowed for
57 high-throughput monitoring and mapping of agricultural ecosystems and has been proven to be
58 convenient and efficient for crop N status monitoring (Kalacska et al., 2015).

59 With the development of UAV technology, it has been widely used in precision agriculture for
60 its low cost, flexibility and high temporal and spatial resolution (Bendig et al., 2015). Monitoring N
61 status using UAVs has been found successful in different crops in previous studies. For example,
62 (Li et al., 2018c) found it held great potential using UAV-based active sensing for monitoring rice
63 leaf N status. An octocopter UAV was used for capturing multi-angular images to estimate the
64 nitrogen content and accumulation of winter wheat at leaf and plant scale, with the highest accuracy
65 obtained for leaf NC from single-angle images (Lu et al., 2019). There are also many studies about
66 N determination using UAV in other crops such as maize (Maresma et al., 2016), winter oilseed rape
67 (Liu et al., 2018) and sorghum (Li et al., 2018b).

68 Typically, several methods including statistical regression techniques alongside physically
69 based models are adopted in phenotyping. The physically based models have not been fully
70 examined for crop N monitoring so far though better transferability can be offered (Wang et al.,
71 2015). A few studies proposed modification of radiative transfer models such as the N-PROSPECT
72 (Yang et al., 2015) or N-PROSAIL (Li et al., 2018a) for monitoring crop N status at leaf or canopy
73 scale. However, the models are restricted to few crops and the parameters are complex and not
74 convenient to obtain in agricultural practice (Verrelst et al., 2015; Yang et al., 2015), limiting their
75 use in crop N monitoring. Actually, previous works on N diagnosis in crops predominantly adopted
76 statistical regression techniques. Different spectral features were used to establish parametric or

77 nonparametric linkages with crop physiological and biochemical traits including NC and many other
78 N related indicators. A range of studies has used VIs to construct N estimation empirical regression
79 models and achieve great performance (Song et al., 2016; Tilly and Bareth, 2019). Through the
80 combination of different bands, VIs could be sensitive to the differences (e.g., biomass variation
81 among different stages) in crop phenotypes. (Wang et al., 2012) reported an effective approach of
82 leaf N monitoring using three-band VIs both in wheat and rice. (Zhang et al., 2018) constructed the
83 modified simple ratio index, and found it had a great correlation with wheat NUE. Some published
84 VIs were proved to be well correlated with leaf NC of maize and a new optimized red-edge
85 absorption area index was proposed for the estimation of the vertically integrated leaf NC (Wen et
86 al., 2021). However, crop N monitoring based on single VI could be unreliable due to the limited
87 band information of single VI. With the development of numerous algorithms such as parametric
88 regressions, linear nonparametric regression and nonlinear nonparametric regression, one can make
89 full use of the different bands for crop N monitoring based on VIs (Berger et al., 2020). Texture, as
90 an important characteristic for image classification, has been used in the estimation of forest
91 aboveground biomass (Murray et al., 2010; Kelsey and Neff, 2014). Recently, image texture
92 information have been increasingly used for crop monitoring. (Zheng et al., 2019) found that the
93 using the combination of textural information with spectral information derived from UAV-based
94 images could significantly improve the accuracy for rice biomass estimation compared to the use of
95 spectral information alone. (Yue et al., 2019) has also found similar results in winter wheat biomass
96 monitoring. (Zheng et al., 2020) found that the integration of texture information and VIs could
97 significantly improve all N nutrition parameters estimation using multiple linear regression.
98 However, little is known about the feasibility of using image texture information extracted from
99 UAV images for assessing crop NUE indicators.

100 It is well known that crop growth is a dynamic process with constant nitrogen turnover. The
101 operation of nitrogen varies in different growth stages and different organs in crops (Ohyama Takuji,
102 2010). Studies have indicated that different organs could have different effects on the crop spectral
103 features (Li et al., 2015, 2021). However, few investigations under field conditions address the
104 differences of estimated the NC in different organs when using UAV-based multispectral data.
105 Therefore, the main objectives of this study are to (1) evaluate the potential of UAV-based remote
106 sensing images to predict NC in different organs of winter wheat; (2) compare the performance of
107 nitrogen monitoring in winter wheat based on VIs, TFs and the combination of them, in combination
108 with regression algorithms.

109 **2 MATERIALS AND METHODS**

110 **2.1 Study Area and Experimental Design**

111 Field trials were conducted at the Wuqiao Experimental Station of China Agricultural
112 University (37°41'N, 116°37'E) in Hebei Province in the North China Plain (NCP) (Figure 1) within
113 the winter wheat season of 2020 to 2021. NCP belongs to a warm temperate semi-humid continental
114 monsoon climate. The average rainfall, temperature and altitude were about 550 mm, 12.5 °C and
115 18 m. JiMai22 (*Triticum aestivum* L.), one of the most widely grown winter wheat varieties in NCP
116 was used in this study. It was sowed in October 2020 and harvested in June 2021 with a row spacing
117 of 15 cm and a density of $430 \times 10^4 \text{ ha}^{-1}$. The experiment followed a block design and five levels of
118 nitrogen fertilizer treatments were established, including 0 kg N ha⁻¹ (N0), 120 kg N ha⁻¹ (N1), 180
119 kg N ha⁻¹ (N2), 240 kg N ha⁻¹ (N3) and 300 kg N ha⁻¹ (N4). 120 kg P₂O₅ ha⁻¹ and 90 kg K₂O ha⁻¹
120 were applied to the soil as basal dressings and the rest of the field management followed the local

121 crop production standards throughout the winter wheat season. Besides, three replications were
 122 conducted for each treatment, and each plot area was 40 m² (10 m × 4 m).

123 2.2 Data Collection

124 2.2.1 Field Sampling and NC Determination

125 Destructive samplings were performed eight times (dates) during the growth of winter wheat,
 126 including three times in the vegetative growth phase and five times in the reproductive growth phase
 127 of winter wheat (Table 1).

128 Table 1: Cultivar, treatments and data acquisition schedule.

Cultivar	N rate (Kg ha ⁻¹)	UAV Flight Date	Field sampling Date	Growth stage	Zadoks Codes
JiMai22	0 (N0), 80 (N1), 120 (N2), 160 (N3), 200 (N4)	18 April 2021	18 April 2021	Jointing stage (JS)	GS31
		27 April 2021	27 April 2021	Booting stage (BS)	GS40
		5 May 2021	5 May 2021	Heading stage (HS)	GS50
		12 May 2021	12 May 2021	5 Days after flowering (AF5)	GS70
		17 May 2021	17 May 2021	10 Days after flowering (AF10)	GS75
		22 May 2021	22 May 2021	15 Days after flowering (AF15)	GS80
		27 May 2021	27 May 2021	20 Days after flowering (AF20)	GS85
		1 June 2021	1 June 2021	25 Days after flowering (AF25)	GS90

129 Winter wheat plants within an area of 0.06 m² (0.2 m × 0.3 m) of were randomly selected from
 130 each plot and transported back to the laboratory immediately. All plants were separated into different
 131 organs (leaf, stem, spike and grain). The samples of organs were oven-dried for 30 mins at 105 °C
 132 and later at 80 °C to a constant weight. After obtaining the dry matter weight (DMW) of the different
 133 organs, dried organ samples were ground to pass through a 1 mm screen and stored in plastic bags
 134 for further elemental (N) analysis. At the mature stage of wheat, a 1.8 m² area of wheat plants were
 135 randomly harvested from each plot to determine the final yield. The micro-Kjeldahl method (A.,
 136 1982) was used to determine the total N concentration of different organs. Equation (1) was used to
 137 calculate the plant NC. As one of the indicators for crop NUE, the nitrogen agronomic efficiency
 138 (NAE) can be calculated by equation (2).

$$139 \quad PNC = (L_W \times L_N + S_W \times S_N + SP_W \times SP_N) / (L_W + S_W + SP_W) \quad (1)$$

$$140 \quad NAE = (GY_n - GY_0) / NFA \quad (2)$$

141 Where L_W, S_W, P_W were the DMW of leaf, stem and spike, respectively. L_N, S_N, SP_N were the N
 142 concentration of leaf, stem and spike, respectively. And GY_n is the grain yield with N fertilizer
 143 application, GY₀ is the grain yield without N fertilizer application. NFA means the amount of applied
 144 N fertilizers (kg/ha).

145 2.2.2 UAV Image Acquisition

146 The acquisition dates of UAV-based images can be found in Table 1. All UAV flight missions
 147 were carried out at approximately 10:00 am and 14:00 pm on sunny days. DJI Phantom 4 quadcopter
 148 (DJI, Shenzhen, Guangdong, China), which was equipped with a consumer-grade multispectral
 149 camera was used in this study. The camera consists of six sensors, including five monochromatic
 150 sensors and one Red-Green-Blue (RGB) sensor. The spectral resolution of the monochromatic
 151 sensors includes: a blue band with 450 nm center and 16 nm bandwidth, a green band with 560 nm
 152 center and 16 nm bandwidth, a red band with 650 nm center and 16 nm bandwidth, a red-edge band
 153 with 730 nm and 16 nm bandwidth and a near-infrared band with 840 nm and 26 nm bandwidth.

154 More specific parameters of the UAV and the camera are demonstrated in (Wang et al., 2022a).

155 Nine ground control points (GCPs) were evenly placed over the field for subsequent image
156 geometry correction. To record the precise coordinate information of GCPs, a D-RTK 2 high-
157 precision GNSS mobile station (DJI, Shenzhen, Guangdong, China) operating at centimeter-level
158 positioning precision with uninterrupted data transmission was used in this experiment. The UAV
159 was flown over the winter wheat field at an altitude of 25 m above the ground level. All flight
160 missions were conducted using the DJI go pro software (DJI, Shenzhen, Guangdong, China), with
161 the heading and side overlaps of 80% and 70%, respectively. All acquired images were saved in
162 TIFF format on the SD card onboard the UAV.

163 **2.3 Image processing**

164 *2.3.1 Generation of orthophoto maps*

165 We used the Pix4D (Pix4D SA, Lausanne, Switzerland) based on the structure-from-motion
166 (SfM) technique to generate orthophoto images. Following image alignment, matching, mosaicking,
167 sparse point cloud, and dense point cloud constructing, the orthoimages were generated. The ‘Multi-
168 spectral Ag’ template was selected as the processing model for the orthomosaic reflectance images.
169 The coordinates of GCPs were used for orthomosaic georeferencing by manually identifying the
170 points after generating the sparse point cloud. Finally, five georeferenced single-band orthophotos
171 were obtained in each observed stage with the Geo-TIFF format.

172 *2.3.2 Selection and extraction of vegetation index and image texture*

173 Forty-three nitrogen-related VIs (Table S1 in Supplementary Material S1) were screened for
174 further analysis. QGIS (QGIS Version 3.14) was used to calculate the vegetation index maps. We
175 used the function of the “raster calculator” to obtain the VI-maps based on single-band orthophotos
176 generated by Pix4D for each observation stage. Also, eight grey-level co-occurrence matrix
177 (GLCM)-based textures including the mean (Mean), variance (Var), homogeneity (Hom), contrast
178 (Con), dissimilarity (Dis), entropy (Ent), second moment (Sec), and correlation (Cor) (Haralick et
179 al., 1973) were computed using the ENVI software (Exelis Visual Information Solutions, Boulder,
180 Colorado, USA) with the size of moving window of 5×5 and in the direction of 45° for all the five
181 single-band orthophotos (Table S2 in Supplementary Material S1). Next, regions of interest (ROIs)
182 were selected for each plot, and the mean values of the VI-maps and texture maps were extracted
183 using the “Zonal Statistic” function in QGIS.

184 **2.4 Model development and evaluation**

185 *2.4.1 Model calibration*

186 Correlation analysis was performed for the VIs and the nitrogen content of different organs.
187 Meanwhile, to evaluate the performance of the 43 VIs and 40 TFs obtained from the UAV-based
188 images, the Pearson correlations between VIs/TFs and NC of winter wheat were implemented
189 during the vegetative and reproductive growth phase. For further determination optimal
190 combination of multispectral VIs, TFs and regression algorithms for nitrogen prediction, the Partial
191 Least Squares Regression (PLSR) and Random Forest (RF) algorithms were adopted in this study.

192 Partial least squares regression is one of the most used algorithms to search the basic
193 relationship between two matrices (independent and dependent variables), that is, a latent variable
194 method for modeling the covariance structure in these two vector spaces. It has the advantages of
195 being stable, and suitable for small datasets and can avoid multicollinearity. By conducting the one-
196 sigma algorithm (Wold et al., 2001), the optimal number of latent variables was determined. For the

197 evaluation of the contribution of different VIs to the prediction model, the Variable Importance in
198 Projection (VIP) criterion was introduced (Hastie et al., 2005). In general, variables with a VIP score
199 greater than 1 are considered to be more important to the model. Meanwhile, the larger the VIP
200 value obtained by the variable, the greater the contribution of the variable to the model.

201 The random forests algorithm was developed by (Breiman and Cutler, 2012) in 2001. As a
202 typical ensemble algorithm, it is composed of multiple unrelated decision trees, and the final output
203 of the model is jointly determined by each decision tree in the forest. It shows a promising capability
204 to avoid overfitting by sampling the predictor space randomly. The number of decision tree (*ntree*)
205 and the input variables per node (*mtry*) are two key hyperparameters that have great impact for the
206 complexity of RF models (Wang et al., 2019). In this study, they were selected based on the root
207 mean square error (RMSE) with the RF algorithm. Besides, as an effective indicator for evaluating
208 the contribution of variables to the model, the percentage increase in mean squared error (%IncMSE)
209 (Farrés et al., 2015) was used in our research. By using the function of ‘rfPermute’ in RF models,
210 the image feature with great importance for the models can be screened out.

211 All datasets were randomly divided into a training dataset (80%) and a test dataset (20%). The
212 packages “pls” (Mevik and Wehrens, 2007) and “randomForest” (Breiman and Cutler, 2012) were
213 used to construct the prediction models in R programming language in R Studio (R Version 3.6.1).

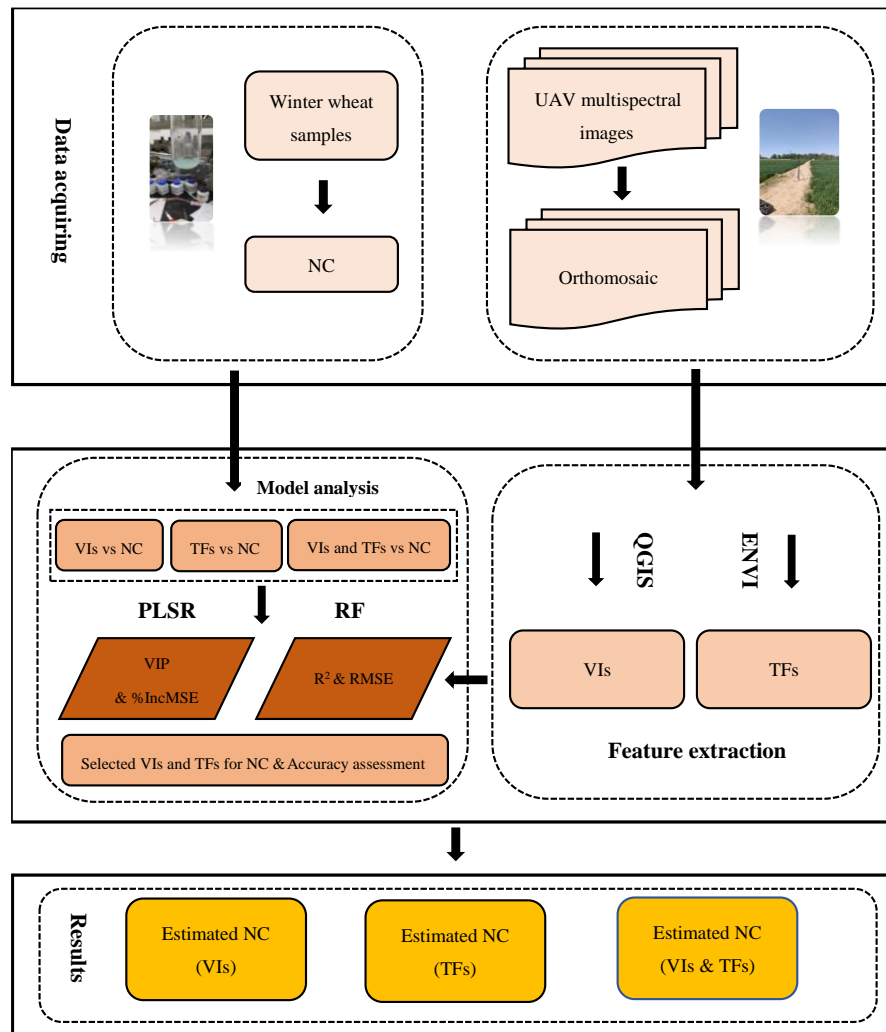
214 2.4.2 Model evaluation

215 The 1:1 line of the estimated and measured nitrogen concentrations were used to assess the
216 fitness of different prediction models. Coefficients of determination (R^2) and root mean square error
217 (RMSE) were selected to evaluate the performances of the different models. Generally, the higher
218 the R^2 and the lower the RMSE, the better the precision and accuracy of the models. These statistical
219 indicators were expressed as equations (3) and (4):

$$220 R^2 = \frac{\sum_{i=1}^n (x_i - \bar{x})(y_i - \bar{y})}{\sqrt{\sum_{i=1}^n (x_i - \bar{x})^2 \sum_{i=1}^n (y_i - \bar{y})^2}} \quad (3)$$

$$221 RMSE = \sqrt{\frac{1}{k} \sum_{i=1}^n (x_i - y_i)^2} \quad (4)$$

222 Where n is the number of samples, i is the i th sample, x_i and y_i stand for the estimated NC
223 values and measured nitrogen concentration values, \bar{x} and \bar{y} stand for the average estimated NC
224 values and measured NC values, respectively. Figure 1 shows the flowchart of the experiment.



225

226 **Figure 1.** The flowchart of the key steps for data collection and analysis in this study.

227

228 3 RESULTS

229

230 3.1 Measured data from destructive sampling

231

232 3.1.1 Descriptive analysis of NC and dry matter weight (DMW)

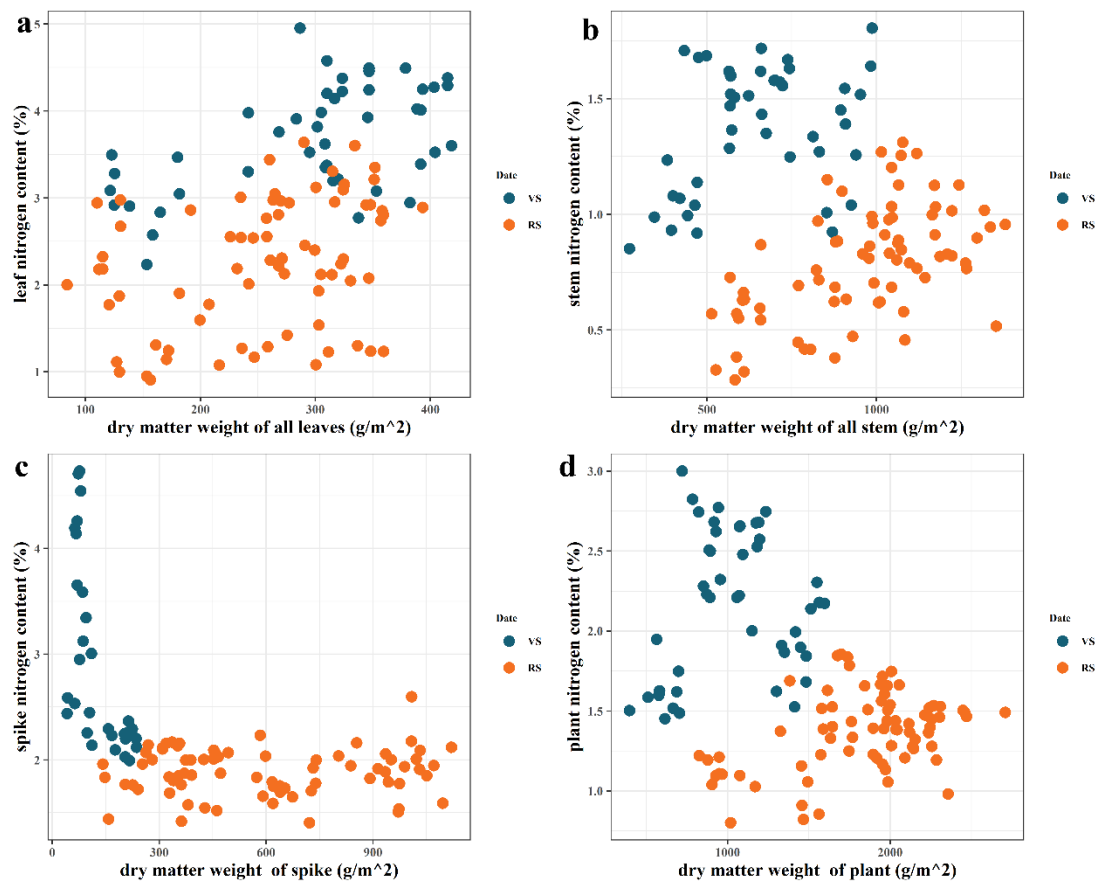
233

234 As shown in Table S3 in Supplementary Material S1, the DMW ranges from 1.22 to 4.18 t/ha
 235 with CV of 31.01% in leaf DWM, from 2.72 to 9.87 t/ha with CV of 39.71% in stem DMW, from
 236 0.42 to 2.37 t/ha with CV of 51.53% in spike DMW, and from 3.97 to 15.96 t/ha with CV of 31.71%
 237 in plant DMW during the vegetative growth phase. For the reproductive growth phase, leaf-, stem-,
 238 spike-, grain- and plant DWM ranges from 0.84 to 3.93 t/ha, 5.14 to 13.80 t/ha, 1.42 to 11.20 t/ha,
 239 0.26 to 8.14 t/ha and 8.26 to 27.08 t/ha, respectively, with CV of 30.76%, 23.44%, 47.86%, 74.41%
 240 24.06%.

241

242 Nitrogen content (NC) varies from 2.24% to 4.95%, 0.85% to 1.81%, 1.99% to 4.73%, 1.45%
 243 to 3.00% in the leaf, stem, spike and plant, respectively, with CV of 16.84%, 19.48%, 31.01% and
 244 20.86% during the vegetative growth phase. For the reproductive growth phase, the leaf, stem, spike,
 grain and plant NC varies from 0.91% to 3.64%, 0.29% to 1.31%, 1.41% to 2.60%, 1.62% to 3.06%,
 and 0.80% to 1.85%, respectively, with CV of 33.41%, 31.10%, 12.00%, 15.04% and 17.78%. It
 can also be found that the variation of leaf NC and stem NC in the reproductive growth phase was
 greater than that in the vegetative growth phase (Table S3), which was opposite with the variation
 trend of spike NC and plant NC in the vegetative and reproductive growth phases.

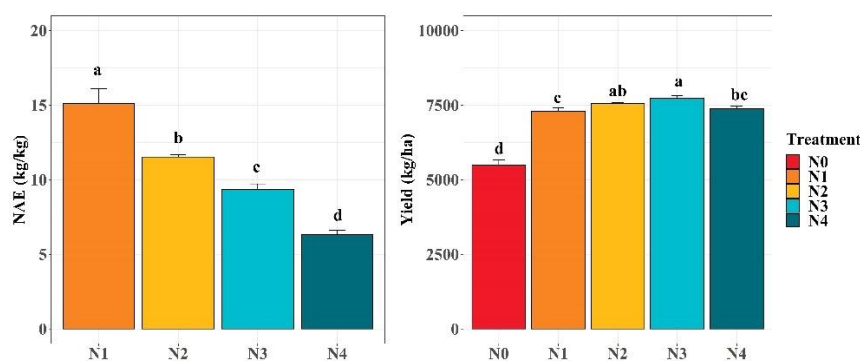
245 Figure 2 shows the relationship between the DMW of leaf, stem, spike and plant and the
 246 corresponding NC values for the vegetative and reproductive growth phases. Except for the leaf NC,
 247 NC in the stem, spike and whole plant decrease as DMW increases due to the dilution effect of N
 248 as described in (Lemaire et al., 2008).



249
 250 **Figure 2.** Winter wheat DMW (g/m^2) vs. winter wheat nitrogen content in the vegetative and
 251 reproductive growth phases; (a) leaf DMW and leaf NC; (b) stem DMW and stem NC; (c) spike
 252 DMW and spike NC; (d) plant DMW and plant NC. VS and RS means the vegetative and
 253 reproductive growth phases.

254 *3.1.2 Yield and nitrogen agronomic efficiency (NAE)*

255 Figure 3 depicts the average yield and the corresponding NAE for each N treatment in the
 256 experiment. The highest yield was observed in the N3 treatment, whereas the lowest yield was
 257 observed in the N0 treatment. NAE decreased significantly along with the increase of N fertilizer
 258 inputs.



259

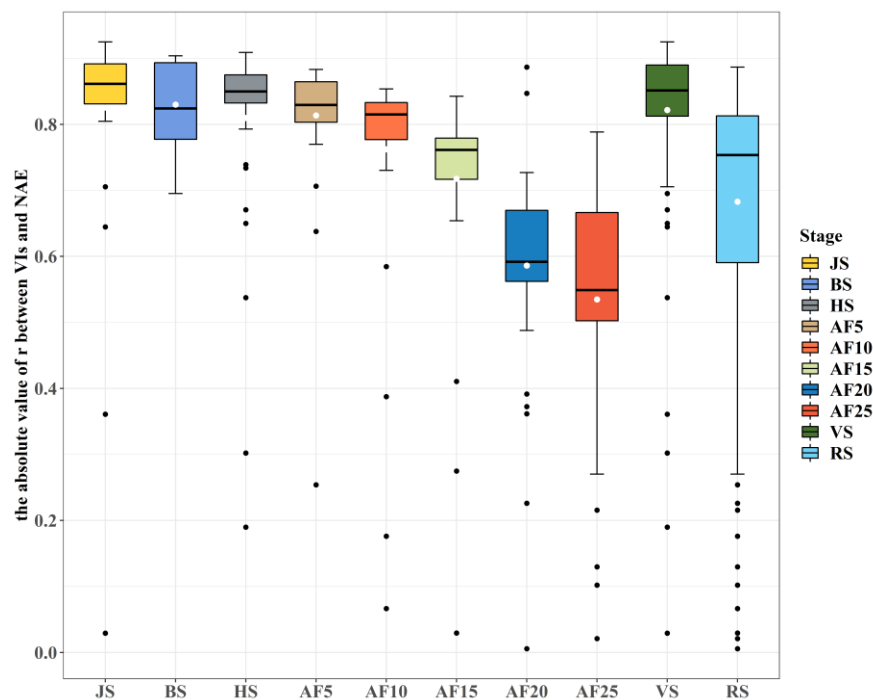
260 **Figure 3.** Yield and NAE of each treatment of N. The different small letters indicate significant
261 differences between treatments.

262 3.2 Correlation between image features vs. N-related indicators

263 Table S4 in Supplementary Material S1 showed the top 5 most relevant VIs and TFs for NC
264 monitoring of winter wheat. In the vegetative growth phase, the RGBVI, MCARI, MCARI2 and
265 RGBVI, were the best correlated VIs for leaf, stem, spike and plant NC, respectively, with r of 0.75,
266 0.80, 0.60 and 0.75. The Reg_mean ($r = -0.85$), G_cor ($r = -0.84$), R_con ($r = 0.32$) and Reg_mean
267 ($r = -0.86$) was the best correlated TFs for leaf, stem, spike and plant NC monitoring. In reproductive
268 growth phase, the GOSAVI and R_ho (with r of 0.88 and 0.84), MSR-REG and G_mean (with r of
269 0.82 and -0.81), DVI-REG and Reg_mean (with r of 0.56 and -0.64), RTVI-CORE and G_mean
270 (with r of 0.71 and -0.58) and CVI and Reg_mean (with r of 0.77 and -0.79) yield the highest r with
271 leaf, stem, spike, grain and plant NC (See detail in Supplementary Material S2).

272 In general, most of VIs were found to be positively correlated with NC, while most of TFs
273 were negatively correlated with NC. Among all the organs and the whole plant, it was obvious that
274 the correlation between spike NC and image features was the lowest.

275 Figure 4 shows the absolute value of the r between VIs and NAE in different growth stages. It
276 is clear that the VIs derived from our UAV images can reflect the change of NAE to a certain extent,
277 and the correlation decreases with the winter wheat growth in general.

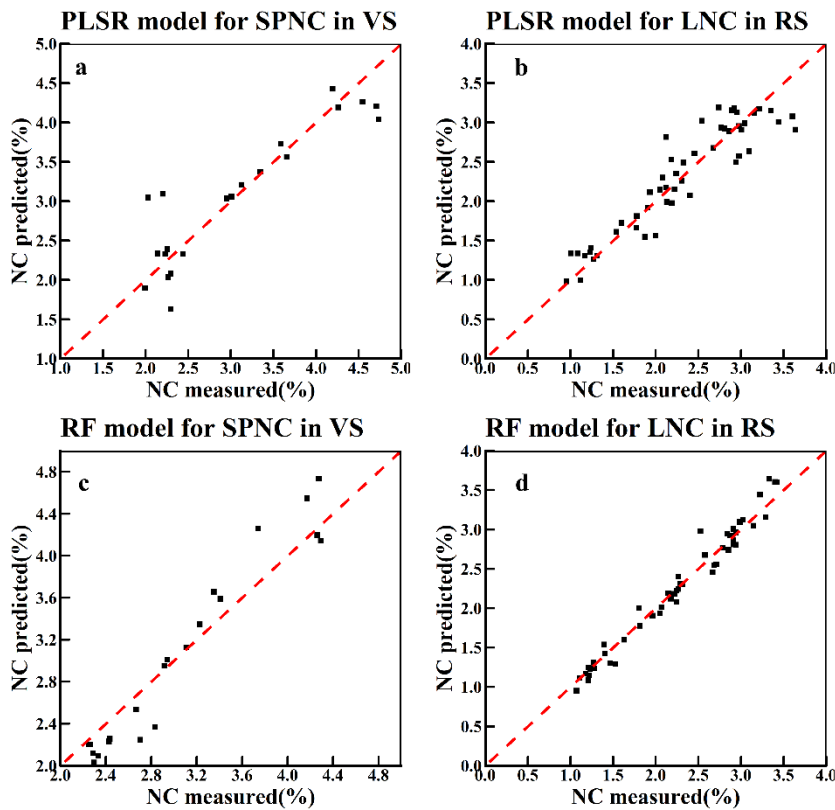


278 **Figure 4.** Variation of the absolute value of the r between VIs and NAE in different growth stage.
279 The white dots in each box represent the mean value of the absolute value of the r , and the black
280 dots represent outliers. JS, BS and HS are jointing, booting and heading stage, respectively. And
281 AF5, AF10, AF15, AF20 and AF25 means 5, 10, 15, 20 and 25 days after flowering. VS and RS
282 refer to the vegetative and reproductive growth phases, respectively.
283

284 3.3 PLSR and RF models using VIs for nitrogen content estimation

285 As shown in Table 2, during the vegetative growth phase, the PLSR model obtained the highest
286 R^2 in spike NC estimating both in training and testing sets but the RMSEs were also generally larger
287 than the ones in the PLSR models. For other organs or the whole plant, there were no obvious

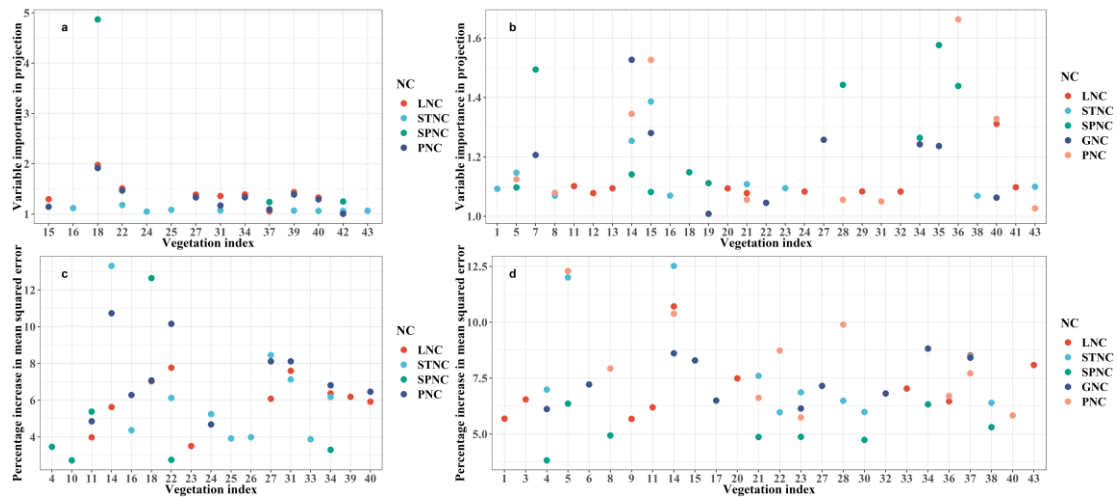
288 differences in the estimation during the vegetative growth phase ($R^2 = 0.74 - 0.77$, $RMSE = 0.13 -$
289 0.30 in training, $R^2 = 0.57 - 0.76$, $RMSE = 0.14 - 0.39$ in testing). Our RF model in the vegetative
290 growth phase allowed the best prediction for spike and plant NC, respectively, in the training and
291 testing sets. Similar to the PLSR model in the vegetative growth phase, the prediction of NC by the
292 RF model did not show differences between different organs in wheat or the whole plant ($R^2 = 0.91$
293 $- 0.94$, $RMSE = 0.07 - 0.26$ in training, $R^2 = 0.73 - 0.82$, $RMSE = 0.13 - 0.50$ in testing). Figure 5
294 shows the PLSR and RF models that had the best overall performance in the vegetative and
295 reproductive growth phases.



296
297 **Figure 5.** The PLSR and RF models which performed best in vegetative and reproductive growth
298 phases using VIs only. (a) the SPNC PLSR model in VS. (b) the LNC PLSR model in RS. (c) the
299 SPNC RF model in VS. (d) the LNC RF model in RS.

300 Figure 6 showed the top 10 important VIs for NC estimation models. Among all the NC of
301 different organs or the whole plant in the vegetative growth phase, MCARI2 was found to be the
302 most important VI for leaf NC ($VIP = 1.98$), spike NC ($VIP = 4.87$) and plant NC ($VIP = 1.92$) in
303 PLSR models. MTCI was the 2nd most important VI for leaf NC ($VIP = 1.51$) and plant NC (VIP
304 $= 1.47$) and was also found to be the most important VI for stem NC ($VIP = 1.18$).

305 As for the RF models in the vegetative growth phase, MTCI, GRVI, MCARI2 and GRVI with
306 contributed most to the leaf-, stem-, spike- and plant NC estimations, respectively, with
307 the %IncMSE of 10.73, 13.31, 12.64 and 10.73 (Figure 6). Also, MCARI2 and MTCI also played
308 an important role in the RF models, which had similarly great performance in the PLSR models
309 during the vegetative growth.



310

311 **Figure 6.** Top 10 important VIs for the NC monitoring of different organs and the whole plant
 312 selected by different models. (a) the TOP 10 important VIs for NC monitoring in vegetative growth
 313 phase selected by PLSR. (b) the TOP 10 important VIs for NC monitoring in the reproductive
 314 growth phase selected by PLSR. (c) the TOP 10 important VIs for NC monitoring in the vegetative
 315 growth phase selected by RF. (d) the TOP 10 important VIs for NC monitoring in the reproductive
 316 growth phase selected by RF. LNC, STNC, SPNC, GNC and PNC are leaf, stem, spike, grain and
 317 plant NC, respectively.

318 For the reproductive growth phase, the VIs that yielded great performance in the NC prediction
 319 models differed. In the PLSR models. TCARI/OSAVI, LCI, SAVI-GREEN, GRVI and S-CCCI have
 320 been found to be the best VIs for leaf, stem, spike, grain and plant NC, respectively, with the VIP of
 321 1.31, 1.37, 1.58, 1.52 and 1.66. In the RF models, GRVI contributed most to the leaf- and stem NC
 322 predictions (%IncMSE = 10.71 and 12.52), CVI contributed most to spike and plant NC (%IncMSE
 323 of 6.36 and 12.30), and SAVI contributed most for grain NC (%IncMSE = 8.82). Besides, it also
 324 indicated that the VIs screened out in the vegetative growth phase are more consistent, while weak
 325 consistency of the top 10 VIs in the reproductive growth phase (Figure 6). Furthermore, we have
 326 also counted the total number of VIs selected by the PLSR and RF models in different growth phases.
 327 Table S4 shows that more VIs have been selected by RF models in the reproductive growth phase
 328 of winter wheat approximately (See detail in Supplementary Material S3).

329 **Table 2.** Nitrogen content estimates using 43 vegetation indices.

Growth phase	Part of winter wheat	Data set	PLSR		RF	
			R ²	RMSE	R ²	RMSE
Vegetative growth phase	Leaf	Training set	0.77	0.30	0.91	0.18
		Testing set	0.57	0.39	0.82	0.38
	Stem	Training set	0.74	0.13	0.93	0.07
		Testing set	0.76	0.14	0.78	0.13
	Spike	Training set	0.82	0.40	0.94	0.26
		Testing set	0.85	0.39	0.73	0.50
	Plant	Training set	0.75	0.23	0.93	0.12
		Testing set	0.63	0.26	0.82	0.23
	Leaf	Training set	0.86	0.27	0.97	0.13

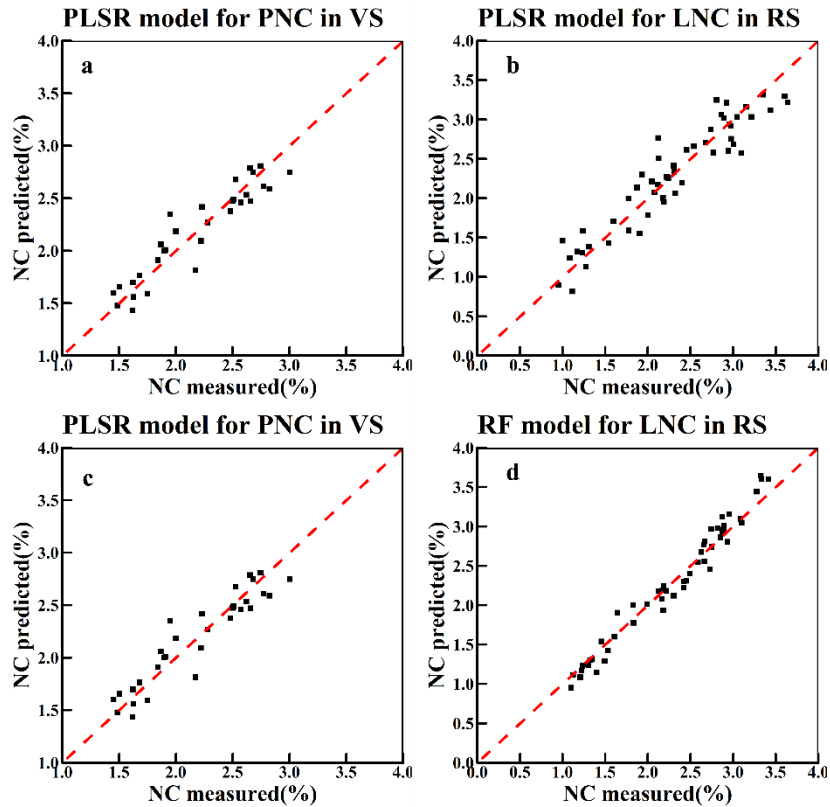
Reproductive growth phase	Stem	Testing set	0.82	0.35	0.84	0.30
		Training set	0.77	0.12	0.96	0.06
	Spike	Testing set	0.64	0.15	0.77	0.14
		Training set	0.52	0.16	0.89	0.09
	Grain	Testing set	0.31	0.15	0.48	0.16
		Training set	0.72	0.20	0.93	0.11
	Plant	Testing set	0.44	0.23	0.55	0.25
		Training set	0.79	0.11	0.95	0.06
		Testing set	0.62	0.15	0.74	0.13

330

331 **3.4 PLSR and RF models using texture features for nitrogen content estimation**

332 In Table 3, it can be found that during the vegetative growth phase, both PLSR ($R^2 = 0.84$,
333 RMSE = 0.16) and RF ($R^2 = 0.97$, RMSE = 0.06) model performed the best for plant NC estimation
334 in the training set. And for leaf and spike NC estimation, both PLSR and RF models achieved great
335 performance with R^2 above 0.79, RMSE below 0.28 in the training set and R^2 above 0.53, RMSE
336 below 0.35 in the testing set. Besides, the results also showed that it was more stable for the
337 prediction of leaf NC than stem NC since the worse performance of both PLSR and RF models in
338 the testing set.

339 In the reproductive growth phase, the performance of the PLSR ($R^2 = 0.88$, RMSE = 0.25 in
340 training, $R^2 = 0.88$, RMSE = 0.32 in testing) and RF ($R^2 = 0.97$, RMSE = 0.14 in training, $R^2 = 0.76$,
341 RMSE = 0.38 in testing) models for the leaf NC prediction were improved. However, the
342 performance of the PLSR ($R^2 = 0.57$, RMSE = 0.16 in training and $R^2 = 0.16$, RMSE = 0.18 in
343 testing) and RF ($R^2 = 0.91$, RMSE = 0.09 in training, $R^2 = 0.31$, RMSE = 0.19 in testing) models
344 for the spike NC prediction was worse than that in the vegetative growth phase. For plant and stem
345 NC monitoring, no significant differences were found between two different stages. Besides, the
346 prediction of grain NC has achieved fairly good performance in the training set though it did not
347 allow great performance in the testing set. We can find the PLSR and RF models with the best
348 overall performance in the vegetative and reproductive growth phases in figure 7.

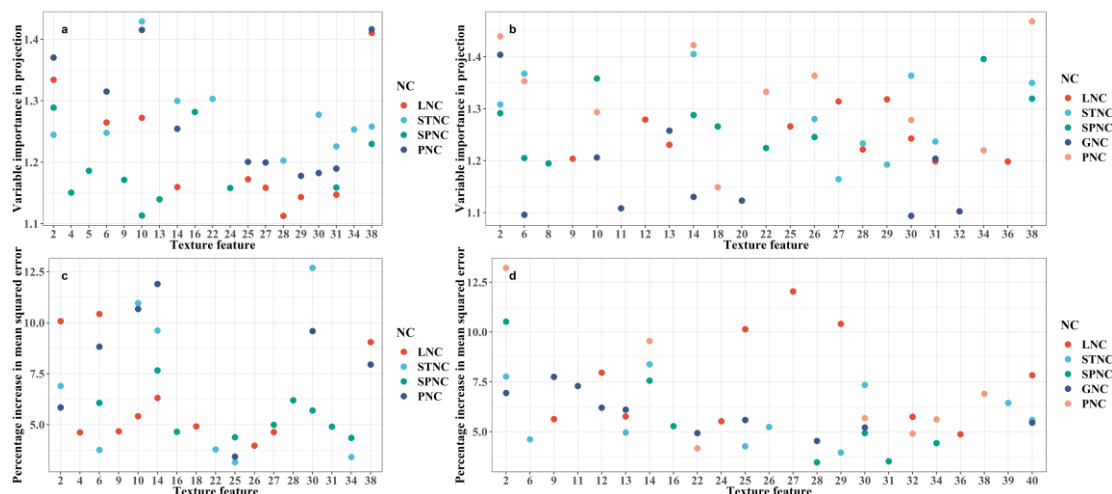


349

350 **Figure 7.** The PLSR and RF models which performed best in vegetative and reproductive growth
351 phases using TFs only. (a) the PNC PLSR model in VS. (b) the LNC PLSR model in RS. (c) the
352 PNC RF model in VS. (d) the LNC RF model in RS.

353 Figure 8 shows the top 10 important TFs for NC estimation models except for the RF models
354 for spike and plant NC for there were fewer than 10 TFs were screened. In the vegetative growth
355 phase, The best TF for leaf, stem, spike and plant NC were Reg_mean (VIP = 1.41), G_cor (VIP =
356 1.43), B_cor (VIP = 1.29) and Reg_mean (VIP = 1.42) for the PLSR models. For RF models,
357 B_mean with %IncMSE of 10.43, R_mean with %IncMSE of 12.69, G_mean with %IncMSE of
358 7.66 and G_mean with %IncMSE of 11.90 was the best TFs for the estimating of leaf, stem, spike
359 and plant NC, respectively. In the reproductive growth phase, for PLSR models, R_ho, G_mean,
360 Reg_cor, B_cor and Reg_mean have been found to be the best TFs for leaf, stem, spike, grain and
361 plant NC, respectively, with the VIP of 1.32, 1.41, 1.40, 1.40 and 1.47. In contrast in the RF models,
362 R_dis, G_mean, G_con and contributed the most to the leaf-, stem-, and grain NC predictions,
363 respectively, with the %IncMSE of 12.04, 8.38 and 7.75. B_cor performed the best for spike and
364 plant NC predictions, respectively, with %IncMSE of 10.52 and 13.22. Furthermore, the result also
365 indicated that the TFs of mean and cor accounted for a relatively large proportion of the variations
366 in both PLSR and RF models.

367 Table S5 shows the number of TFs selected by the PLSR and RF models in different growth
368 phases. It can be found that more TFs were selected by the PLSR models than the RF models.
369 Meanwhile, by counting the TFs screened by the two models, it was found that almost all the
370 important TFs screened out by the models were based on the bands of R, G and B instead of NIR
371 and REG bands (See detail in Supplementary Material S2).



372

373 **Figure 8.** Top 10 important TFs for the NC monitoring of different organ and the whole plant
 374 selected by different models. (a) the TOP 10 important TFs for NC monitoring in vegetative growth
 375 phase selected by PLSR. (b) the TOP 10 important TFs for NC monitoring in reproductive growth
 376 phase selected by PLSR. (c) the TOP 10 important TFs for NC monitoring in vegetative growth
 377 phase selected by RF. (d) the TOP 10 important TFs for NC monitoring in reproductive growth
 378 phase selected by RF. LNC, STNC, SPNC, GNC and PNC are leaf, stem, spike, grain and plant NC,
 379 respectively.

380 Table 3. Nitrogen content estimates using 40 texture features.

Growth stage	Part of winter wheat	Data set	PLSR		RF	
			R ²	RMSE	R ²	RMSE
Vegetative growth stage	Leaf	Training set	0.79	0.28	0.94	0.14
		Testing set	0.72	0.31	0.87	0.35
	Stem	Training set	0.81	0.11	0.96	0.06
		Testing set	0.53	0.21	0.77	0.13
	Spike	Training set	0.57	0.34	0.97	0.18
		Testing set	0.60	0.44	0.94	0.23
	Plant	Training set	0.87	0.16	0.97	0.08
		Testing set	0.72	0.24	0.90	0.17
Reproductive growth stage	Leaf	Training set	0.88	0.25	0.97	0.14
		Testing set	0.88	0.32	0.76	0.38
	Stem	Training set	0.73	0.13	0.94	0.07
		Testing set	0.76	0.12	0.84	0.13
	Spike	Training set	0.57	0.16	0.91	0.09
		Testing set	0.16	0.18	0.31	0.19
	Grain	Training set	0.66	0.23	0.93	0.12
		Testing set	0.26	0.28	0.40	0.27
Plant	Training set	0.74	0.13	0.94	0.06	
	Testing set	0.68	0.14	0.74	0.13	

381

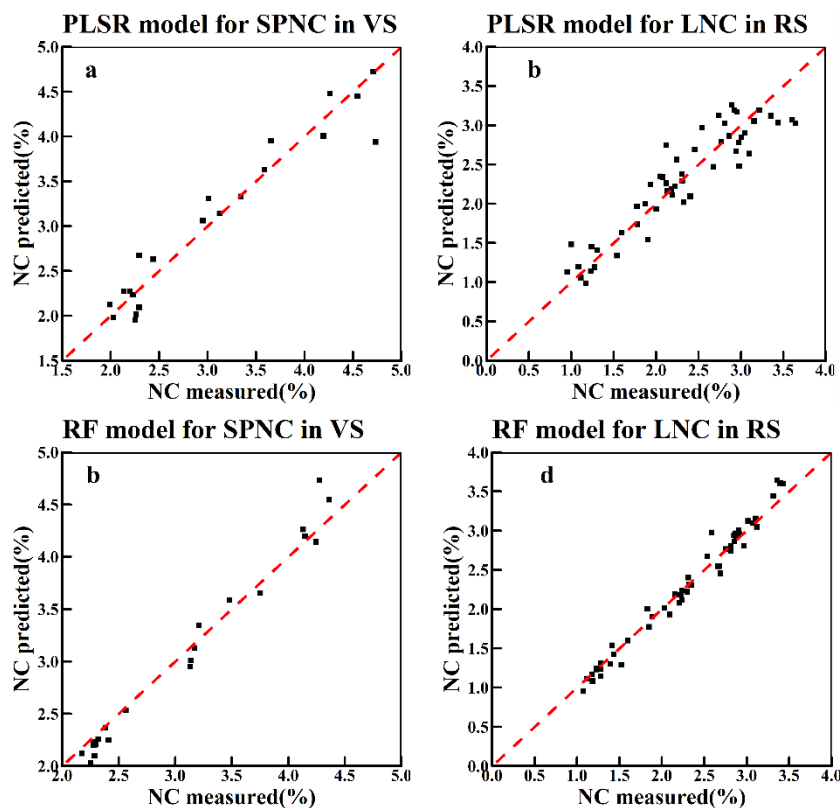
3.5 PLSR and RF models using the combination of VIs and texture features for nitrogen

382

content estimation

383 Table 4 showed that the combination of image VIs and TFs did improve the monitoring
384 accuracy of NC in winter wheat to a certain extent, but the effect was not significant. Among all the
385 models in the vegetative growth phase, the estimation for spike NC has allowed great performance
386 in both PLSR ($R^2 = 0.93$, RMSE = 0.25 in training and $R^2 = 0.77$, RMSE = 0.33 in testing) and RF
387 ($R^2 = 0.98$, RMSE = 0.16 in training and $R^2 = 0.94$, RMSE = 0.23 in testing) models. And better
388 results have been achieved for plant NC monitoring than leaf stem NC monitoring ($R^2 = 0.82 - 0.87$,
389 RMSE = 0.06 - 0.26 in the training set, $R^2 = 0.52 - 0.94$, RMSE = 0.17 - 0.40 in testing set).

390 In the reproductive growth phase, the worst performance was obtained when estimating spike
391 NC ($R^2 = 0.56$, RMSE = 0.16 in the training set and $R^2 = 0.24$, RMSE = 0.17 in the testing set for
392 PLSR model and $R^2 = 0.91$, RMSE = 0.08 in the training set and $R^2 = 0.43$, RMSE = 0.17 in the
393 testing set for RF model). The performance of grain NC was also not so satisfactory in testing set,
394 with R^2 of 0.41 and RMSE of 0.24 in the PLSR model and R^2 of 0.43 and RMSE of 0.17 in the RF
395 model. Apart from that, the best performance was achieved in leaf NC prediction with the highest
396 R^2 of 0.86 in PLSR model and 0.98 in RF model. Figure 9 shows the PLSR and RF models with the
397 best overall performance in the vegetative and reproductive growth phases.

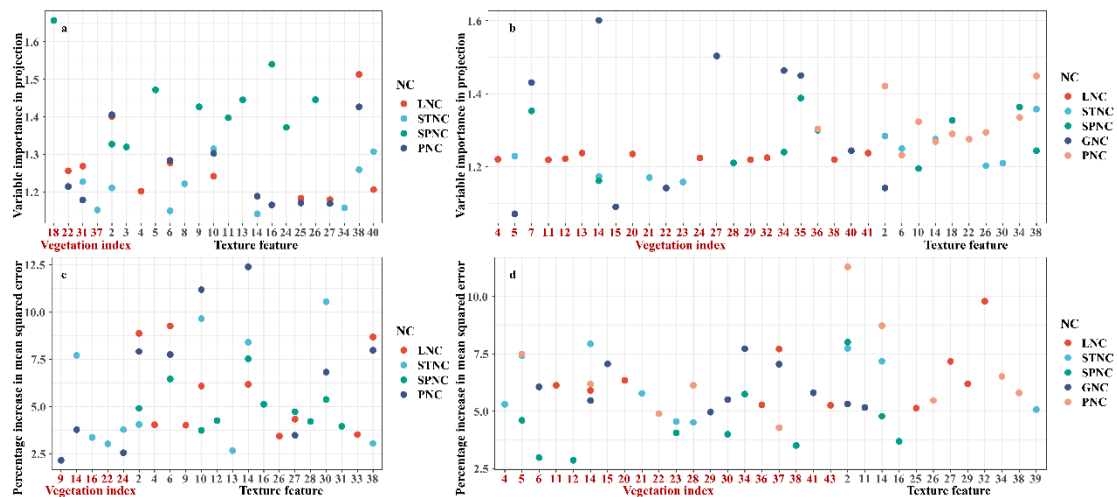


398

399 **Figure 9.** The PLSR and RF models which performed best in vegetative and reproductive growth
400 phases using TFs only. (a) the SPNC PLSR model in VS. (b) the LNC PLSR model in RS. (c) the
401 SPNC RF model in VS. (d) the LNC RF model in RS.

402 Figure 10 shows the TOP 10 selected features based on the PLSR and RF models. In the
403 vegetative growth, the feature with the highest VIP was Reg_mean (VIP = 1.51) for leaf NC, G_cor
404 (VIP = 1.32) for stem NC, MCARI2 (VIP = 1.66) for spike NC and Reg_mean (VIP = 1.43) for
405 plant NC in PLSR model. In RF model, B_mean with %IncMSE of 9.26, R_mean with %IncMSE
406 of 10.54, G_mean with %IncMSE of 7.53 and 12.39 was the best feature for leaf, stem, spike and
407 plant NC. In the reproductive growth stage, GOSAVI, Reg_mean, SAVI-GREEN, GRVI and

408 Reg_mean (with VIP of 1.24, 1.36, 1.39, 1.60 and 1.45) contributed most to the leaf, stem, spike,
 409 grain and plant NC in PLSR models. R_var, GRVI, B_cor, SAVI and B_cor (with %IncMSE of 9.79,
 410 7.94, 8.01, 7.72 and 11.29) contributed most to the corresponding NC estimation in RF models.
 411 Compared with the best image features selected in different growth phases of winter wheat, it also
 412 reflected that the TFs could be more suitable for the monitoring of NC of winter wheat in general.
 413 As for the total number of image features (VIs and TFs) selected by the PLSR and RF models in
 414 different growth phases. For all the PLSR and RF models except for STNC, more TFs was screened
 415 than VIs in the vegetative growth phase. Interestingly, in the reproductive growth phase, more VIs
 416 were screened out than TFs in all the PLSR and RF models except for SPNC, which was different
 417 from the characteristics of in the vegetative growth phase (See detail in Supplementary Material S2).



418
 419 **Figure 10.** Top 10 important image features (VIs and TFs) for the NC monitoring of different organs
 420 and the whole plant selected by different models. (a) the TOP 10 important image features for NC
 421 monitoring in the vegetative growth phase selected by PLSR. (b) the TOP 10 important image
 422 features for NC monitoring in the reproductive growth phase selected by PLSR. (c) the TOP 10
 423 important image features for NC monitoring in vegetative growth phase selected by RF. (d) the TOP
 424 10 important image features for NC monitoring in the reproductive growth phase selected by RF.
 425 LNC, STNC, SPNC, GNC and PNC are leaf, stem, spike, grain and plant NC, respectively.

426 Table 4: Nitrogen content estimates using the combination of vegetation indices and texture features.

Growth phase	Part of winter wheat	Data set	PLSR		RF	
			R ²	RMSE	R ²	RMSE
Vegetative growth phase	Leaf	Training set	0.83	0.26	0.95	0.14
		Testing set	0.54	0.40	0.87	0.35
	Stem	Training set	0.82	0.11	0.96	0.06
		Testing set	0.52	0.20	0.80	0.12
	Spike	Training set	0.93	0.25	0.98	0.16
		Testing set	0.77	0.33	0.94	0.23
	Plant	Training set	0.86	0.17	0.97	0.08
		Testing set	0.69	0.23	0.90	0.17
	Leaf	Training set	0.86	0.27	0.98	0.12
	Testing set	0.85	0.31	0.83	0.32	

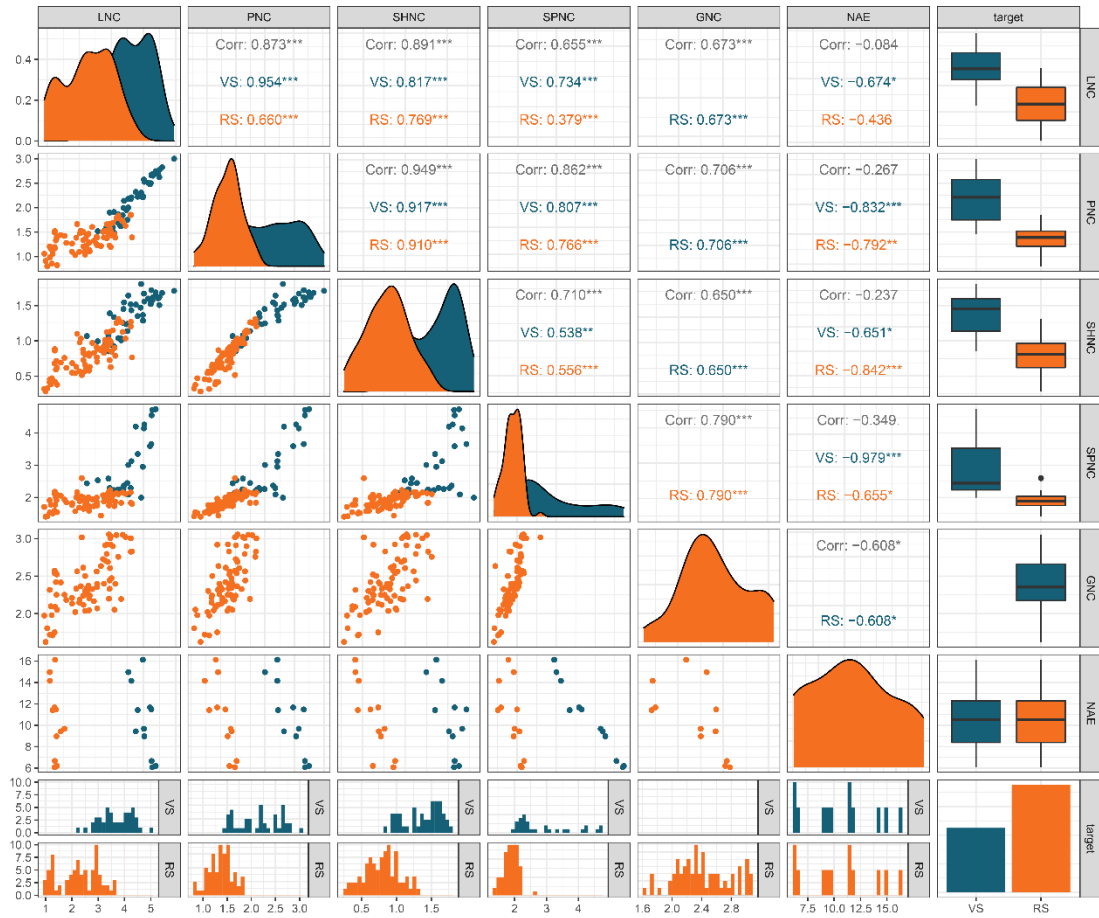
Reproductive growth phase	Stem	Training set	0.79	0.11	0.95	0.06
		Testing set	0.75	0.13	0.85	0.12
	Spike	Training set	0.56	0.16	0.91	0.08
		Testing set	0.24	0.17	0.43	0.17
	Grain	Training set	0.78	0.18	0.93	0.11
		Testing set	0.41	0.24	0.58	0.23
	Plant	Training set	0.81	0.11	0.96	0.06
		Testing set	0.74	0.13	0.76	0.12

427 **4 Discussion**

428 *4.1 UAV-based predictions of nitrogen content in organs and whole plants of winter wheat*

429 In this study, during vegetative and reproductive growth phases, not only the correlation
430 between image features (VIs and TFs) and NC of winter wheat were analyzed, but also the
431 corresponding PLSR and RF models were constructed for the different organs or the whole plant of
432 winter wheat. As found in several preview studies (Zheng et al., 2018; Fu et al., 2020), the leaf and
433 plant NC can be well estimated using VIs or TFs derived from UAV-based images. Our study has
434 also shown great performance of both types of variables for leaf and plant NC predictions during
435 the vegetative and reproductive growth phases. It is worth noting that these variables extracted from
436 the images obtained from the UAV have the capability of estimating the stem, spike and grain NC.

437 It is worth noting that the spike NC always yielded the lowest correlations with VIs and TFs
438 when compared to other organs or the whole plant (Table 3) and, that the predictions for spike NC
439 were not as satisfactory as that for other organs. In contrast, the leaf-, stem- and plant NC were
440 highly correlated in different growth stages, especially in the reproductive growth phase (Figure 11).
441 The relatively low correlations in the vegetative growth phase suggest that the rapid changes in
442 canopy structure during the vegetative growth phase constrained the predictions for leaf, stem and
443 plant NC (Yu et al., 2014). In this study, the VIs and TFs were derived from the delineated subplots
444 (about 30 m²), which reflected the spectral reflectance as a response to the crop canopy variations.
445 Compared to spikes, it is certain that, in orthophotos acquired by the UAV, leaves contributed
446 relatively large to the canopy spectrum (Liu et al., 2017; Yang et al., 2021), which may explain the
447 relatively weak correlations with the extracted VIs and TFs and the relatively high predictions errors
448 (RMSE) for spike NC.



449

450 **Figure 11.** Correlation between nitrogen content and NAE from different organs or the whole plant
 451 of winter wheat. LNC, STNC, SPNC, GNC and PNC are leaf, stem, spike, grain and plant NC,
 452 respectively. NAE is the nitrogen agronomic efficiency. VS and RS means vegetative and
 453 reproductive growth phases. NAE are correlated with the NC of different organs or the whole plant
 454 obtained from two stages (booting and heading stage) in VS, and five stages (AF5, AF10, AF15,
 455 AF20, AF25) in RS.

456 *4.2 Comparisons between the vegetative and reproductive growth phases*

457 Many studies have raised the importance of growth stage on crop agronomic parameters
 458 monitoring (Xue et al., 2004; Li et al., 2010; Wang et al., 2019) found the leaf and plant NC could
 459 be well predicted during the vegetative growth phase including tillering, jointing, booting and
 460 heading stages of rice. Similar studies revealed the monitoring performance of leaf NC for winter
 461 wheat in the reproductive growth phase could be worse than it is performed in vegetative growth
 462 phase (Zheng et al., 2018; Ge et al., 2021; Wang et al., 2022b).

463 In contrast, our results showed inconsistency regarding the best growth stages for leaf NC
 464 prediction. Based on our PLSR and RF models, better prediction performance could be achieved for
 465 predicting leaf NC in the reproductive growth phase though predicting leaf NC in the vegetative
 466 growth phase was also successful. This is attributed to the fact that the unclosed canopy and soil
 467 would be the confusing factors for canopy reflectance in the early vegetative growth phase (Li et
 468 al., 2010). Also, the large variations in biomass over early growth stages will also be responsible for
 469 the worse performance of leaf NC prediction (Yu et al., 2013). In addition, the prediction of spike
 470 NC was found to have the opposite trend compared to the leaf NC, i.e., the vegetative growth phase

471 allowed the best prediction of spike NC. As the reproductive organ of winter wheat, the spike acts
472 as a major photosynthetic organ during the grain filling and has great relevance for plant nitrogen
473 assimilation (Sanchez-Bragado et al., 2014; Vicente et al., 2018). Recent studies have revealed that
474 spikes have certain effects on canopy reflectance spectra, though the complexity of canopy structure,
475 plant density and morphoanatomical and compositional characteristics of spikes in response to
476 canopy spectra still needs to be investigated (Li et al., 2015; Vergara-Diaz et al., 2020).

477 After reaching the reproductive growth phase, the grain appears and becomes the “growth
478 center” of the plant; the N transport mainly happens from the leaf, stem, glume and awn to grain
479 (Maydup et al., 2012; Sanchez-Bragado et al., 2016; Vergara-Diaz et al., 2020). The bad
480 performance of grain NC using PLSR and RF models indicated that grain could be the major
481 confusing factor for the bad performance of spike NC monitoring in the reproductive growth phase,
482 since we could not fully capture the spectral information of grain which was wrapped in glume.
483 Furthermore, compared with leaf, the delayed senescence of spike may also worsen the performance
484 for spike NC monitoring in the reproductive growth phase (Kong et al., 2015; Vicente et al., 2018).
485 However, no significant differences have been found between the two growth phases for the plant
486 ant stem NC predictions, which does not allow us to conclude on which stages could be more
487 suitable for the whole plant and stem NC estimation.

488 *4.3 Comparison between image feature types (VIs and TFs)*

489 Our result has shown that both VIs and TFs can be great features for winter wheat N monitoring.
490 However, inconsistent with the results which were highlighted in crop biomass monitoring (Yue et
491 al., 2019; Zheng et al., 2019), the combination of VIs and TFs didn’t significantly improve the
492 estimation accuracy of NC of winter wheat in our study. Actually, there were a few studies focused
493 on the contribution of the integration of VIs and TFs for crop N monitoring and generally, they
494 concluded that combining VIs and TFs performed better than only using the VIs or TFs, e.g., for
495 leaf and plant NC monitoring (Jia and Chen, 2020; Zheng et al., 2020). The multiple types of VIs
496 can make more extensive use of waveband information and provide more complementary predictors
497 for the NC model construction. Thus, the machine learning algorithms have the ability to integrate
498 and utilize the spectral information contained in VIs, which could be the explanation for the great
499 performance achieved for the combined use of VIs (Wang et al., 2022a). However, probably due to
500 the contrasting correlation patterns observed here - VIs and TF were correlated positively and
501 negatively with NC respectively, the combined use of both types of variables did not improve the
502 predictions of NC.

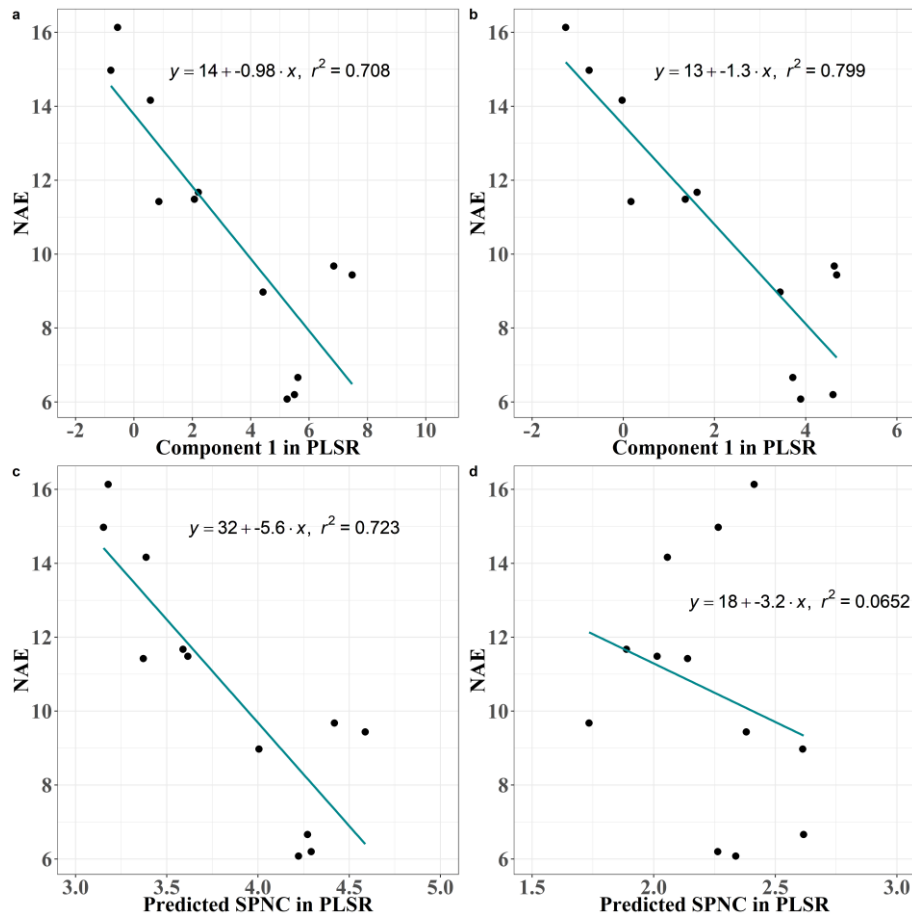
503 By comparing screened image features, there are a few interesting patterns that deserve our
504 attention. Firstly, compared to the image features screened out in the vegetative growth phase
505 (Figures 6, 8, 10), more features with strong consistency were screened out for the PLSR and RF
506 models of different organs in the reproductive growth phase. This could be explained by the
507 complicated canopy structure of winter wheat in the late growth stages, leading to many problems
508 for crop monitoring, such as the saturated VIs (Haboudane et al., 2004). Secondly, among all the
509 top 10 VIs screened out for different organs, most VIs such as MCARI2, MTCI, TCARI,
510 TCARI/OSAVI, SAVI and OSAVI could fall into the ‘soil-line’ VIs and the VIs related to
511 chlorophyll. For example, MCARI2 was reported to be the sensitive VI for the monitoring of N
512 status in the early stage of maize and winter wheat (Nigon et al., 2020). MTCI have also been
513 reported to be the promising spectral index for determining N stress level of potato (Nigon et al.,
514 2015), monitoring the leaf NC of rice (Tian et al., 2011) and estimating the N status of maize (Li et

515 al., 2014). As for the soil-line VIs, lots of studies have demonstrated its' promise for N monitoring
516 (Gabriel et al., 2017; Klem et al., 2018; Guo et al., 2019). The high correlation between N and
517 chlorophyll and the strong ability to minimize soil background influence may be the main reason
518 for the great performance of these indices in the early growth stages. In contrast, the VIs selected in
519 the reproductive growth phase were not as consistent as they were in the vegetative growth phase.
520 Thirdly, the result of selected TFs showed that among all the TFs derived from five different band,
521 more TFs based on R, G and B band were selected by our PLSR and RF models. Also, the texture
522 *mean* and *cor* features accounted for a large proportion in the selected top 10 TFs. It has been know
523 that the mean and cor exhibited great performance in classification tasks (Wan and Chang, 2019).
524 Similar results have been reported for the performance of the texture mean for biomass monitoring
525 in (Fu et al., 2021). The texture mean reflects the degree of regularity of the texture and cor describes
526 the similarity of elements within a line or a row in the GLCM features (Zhu et al., 2022), and thus
527 it has the capability of smoothing the image and minimizing the interference of background. Lastly,
528 although the performance of the combination of VIs and TFs did not show better performance for
529 N monitoring compared with the models based only on VIs and TFs, the top 10 image features
530 filtered by our models based on the combination of VIs and TFs indicated that TFs deserve more
531 attention in the future research since more TFs were selected among the top 10 image features in
532 almost all the models. Overall, these TFs should be further evaluated in future research, such as
533 whether the accuracy of the models can be improved when using the normalized texture index or
534 when monitoring nitrogen in different crop species and varieties.

535 *4.4 UAV-based predictions of N use efficiency*

536 As an important indication for crop N use efficiency, the potential of NAE for crop N status
537 monitoring has not been well evaluated using UAV-based imaging. There were only limited studies
538 reported the attempts on the UAV-based estimation of N use efficiency, which for instance is
539 reflected by the correlation between the UAV-based multispectral traits with NUE (Yang et al., 2020).
540 (Liang et al., 2021) has revealed the capability of using UAV multispectral imagery for the
541 identification of high N use efficiency phenotype in rice. Our results demonstrated that, by only
542 using the latent variables extracted from UAV images, we could predict the NAE (Figure 12),
543 highlighting the prospect of using of UAV-based images to estimate the indicators of NUE. The
544 results of Pearson's correlation analysis (Figure 4) over growth stags also confirm the findings of
545 previous studies that the VIs derived from the multi-temporal images have the potential to forecast
546 the canopy growth dynamics in relation to NUE. Also, the relatively better correlations between NC
547 and NAE in the vegetative growth phase (Figure 11) than in the reproductive growth phase suggest
548 the potential of assessing NUE in the early stages, e.g., for crop variety testing purposes.

549 Furthermore, since the NAE is derived from the yield, the high correlation between VIs and
550 NAE might also be due to the observed better performance for spike NC predictions in the vegetative
551 growth phase. It is worth noting that the application of N fertilizer of winter wheat is mainly in the
552 early growth stages during the vegetative growth phase, and thus the accurate monitoring of wheat
553 N status in the early growth stage will provide more practical implications for wheat N fertilization
554 for improved NUE and reduced environmental costs.



555

556

557

558

559

560

561

562

563

564

565

566

567

568

569

570

571

572

573

574

575

576

577

Figure 12. The performance of using the ‘Component 1’ and the predicted SPNC from the PLSR model in the vegetative growth phase for NAE predicting. (a) the performance of using the component 1 in the PLSR model for NAE predicting in the booting stage; (b) the performance of using the component 1 in the PLSR model for NAE predicting in the heading stage; (c) the performance of using the predicted SPNC in the PLSR model for NAE predicting in booting stage; (d) the performance of using the predicted SPNC in the PLSR model for NAE predicting in heading stage.

563 **5 Conclusions**

In this study, the multi-temporal measured nitrogen content (NC) in different organs or the whole plant of winter wheat obtained by field sampling was associated with the corresponding images acquired by a multi-spectral UAV. Stem-, spike- and plant- NC are found to decrease as dry matter weight (DMW) increased. Positive correlations were found between most of the VIs and NC, while negative correlations were found between most of the TFs and NC. PLSR and RF models successfully employed the VIs, TFs and their combinations to estimate the NC in the whole plant and different organs. PLSR latent variables extracted from the VIs and TFs explained successfully predicted the nitrogen agronomic efficiency (NAE). Although no significant differences were found between the VIs and TFs in their performance in predicting NC, some VIs like MCARI2 and TFs like texture mean were found to perform well in predicting NC. Finally, this study demonstrates that it is feasible to use UAV imaging and PLS/RF models to estimate NC and nitrogen use efficiency both in the vegetative and reproductive growth phases of winter wheat.

576 **DATA AVAILABILITY STATEMENT**

The datasets generated for this study are available on request to the corresponding author.

578 **AUTHOR CONTRIBUTIONS**

579 Experiments were designed by F.W. and K.Y.; F.W., Y.L., L.M., and L.Q performed the flight
580 missions and completed the acquisition of dry matter weight of winter wheat in the field; F.W.
581 compiled the data and conducted the data analysis; W.L. provided software technical support. Z.W.,
582 Y.Z., Z.S. and K.Y. supervised the experiments; F.W. wrote the initial draft of the manuscript and
583 F.L. and K.Y. revised and edited the manuscript. All authors have approved the submitted version
584 of the manuscript.

585 **FUNDING**

586 This work was financially supported by the Key Research Projects of Hebei Province (Grant number:
587 21327003D) and the China Agricultural Research System (CARS301), and the Basic Science
588 Research Fund of China Agricultural University (2020RC037).

589 **ACKNOWLEDGMENTS**

590 We thank the Wuqiao Experimental Station of China Agricultural University for the experiment site
591 and equipment. We are also grateful for Ying Liu, Chenhang Du and Chunsheng Yao for their
592 supports in field sampling. K.Y. appreciates the support by China Agricultural University while he
593 was working at CAU.

594 **References**

- 595 A., L. P. (1982). *Methods of soil analysis. Part 2. Chemical and microbiological properties.*
- 596 Bendig, J., Yu, K., Aasen, H., Bolten, A., Bennertz, S., Broscheit, J., et al. (2015). Combining UAV-
597 based plant height from crop surface models, visible, and near infrared vegetation indices for
598 biomass monitoring in barley. *Int. J. Appl. Earth Obs. Geoinf.* 39, 79–87. doi:
599 10.1016/j.jag.2015.02.012.
- 600 Berger, K., Verrelst, J., Féret, J. B., Wang, Z., Woche, M., Strathmann, M., et al. (2020). Crop
601 nitrogen monitoring: Recent progress and principal developments in the context of imaging
602 spectroscopy missions. *Remote Sens. Environ.* 242, 111758. doi: 10.1016/j.rse.2020.111758.
- 603 Breiman, L., and Cutler, A. (2012). Breiman and Cutler's random forests for classification and
604 regression. *Packag. "randomForest,"* 29. Available at: [https://cran.r-](https://cran.r-project.org/web/packages/randomForest/randomForest.pdf)
605 [project.org/web/packages/randomForest/randomForest.pdf](https://cran.r-project.org/web/packages/randomForest/randomForest.pdf).
- 606 Cao, Q., Miao, Y., Wang, H., Huang, S., Cheng, S., Khosla, R., et al. (2013). Non-destructive
607 estimation of rice plant nitrogen status with Crop Circle multispectral active canopy sensor. *F.*
608 *Crop. Res.* 154, 133–144. doi: 10.1016/j.fcr.2013.08.005.
- 609 Chlingaryan, A., Sukkarieh, S., and Whelan, B. (2018). Machine learning approaches for crop yield
610 prediction and nitrogen status estimation in precision agriculture: A review. *Comput. Electron.*
611 *Agric.* 151, 61–69. doi: 10.1016/j.compag.2018.05.012.
- 612 Cui, Z., Zhang, F., Chen, X., Miao, Y., Li, J., Shi, L., et al. (2008). On-farm evaluation of an in-season
613 nitrogen management strategy based on soil Nmin test. *F. Crop. Res.* 105, 48–55. doi:
614 10.1016/j.fcr.2007.07.008.
- 615 Errecart, P. M., Agnusdei, M. G., Lattanzi, F. A., and Marino, M. A. (2012). Leaf nitrogen
616 concentration and chlorophyll meter readings as predictors of tall fescue nitrogen nutrition status.
617 *F. Crop. Res.* 129, 46–58. doi: 10.1016/j.fcr.2012.01.008.
- 618 Farrés, M., Platikanov, S., Tsakovski, S., and Tauler, R. (2015). Comparison of the variable importance
619 in projection (VIP) and of the selectivity ratio (SR) methods for variable selection and
620 interpretation. *J. Chemom.* 29, 528–536. doi: 10.1002/cem.2736.
- 621 Fu, Y., Yang, G., Li, Z., Song, X., Li, Z., Xu, X., et al. (2020). Winter wheat nitrogen status estimation

- 622 using uav-based rgb imagery and gaussian processes regression. *Remote Sens.* 12, 1–27. doi:
623 10.3390/rs12223778.
- 624 Fu, Y., Yang, G., Song, X., Li, Z., Xu, X., Feng, H., et al. (2021). Improved estimation of winter wheat
625 aboveground biomass using multiscale textures extracted from UAV-based digital images and
626 hyperspectral feature analysis. *Remote Sens.* 13, 1–22. doi: 10.3390/rs13040581.
- 627 Gabriel, J. L., Zarco-Tejada, P. J., López-Herrera, P. J., Pérez-Martín, E., Alonso-Ayuso, M., and
628 Quemada, M. (2017). Airborne and ground level sensors for monitoring nitrogen status in a
629 maize crop. *Biosyst. Eng.* 160, 124–133. doi: 10.1016/j.biosystemseng.2017.06.003.
- 630 Ge, H., Xiang, H., Ma, F., Li, Z., Qiu, Z., Tan, Z., et al. (2021). Estimating plant nitrogen concentration
631 of rice through fusing vegetation indices and color moments derived from UAV-RGB images.
632 *Remote Sens.* 13. doi: 10.3390/rs13091620.
- 633 Guo, C., Tang, Y., Lu, J., Zhu, Y., Cao, W., Cheng, T., et al. (2019). Predicting wheat productivity:
634 Integrating time series of vegetation indices into crop modeling via sequential assimilation.
635 *Agric. For. Meteorol.* 272–273, 69–80. doi: 10.1016/j.agrformet.2019.01.023.
- 636 Haboudane, D., Miller, J. R., Pattey, E., Zarco-Tejada, P. J., and Strachan, I. B. (2004). Hyperspectral
637 vegetation indices and novel algorithms for predicting green LAI of crop canopies: Modeling and
638 validation in the context of precision agriculture. *Remote Sens. Environ.* 90, 337–352. doi:
639 10.1016/j.rse.2003.12.013.
- 640 Hank, T. B., Berger, K., Bach, H., Clevers, J. G. P. W., Gitelson, A., Zarco-Tejada, P., et al. (2019).
641 *Spaceborne Imaging Spectroscopy for Sustainable Agriculture: Contributions and Challenges*.
642 Springer Netherlands doi: 10.1007/s10712-018-9492-0.
- 643 Haralick, R. M., Dinstein, I., and Shanmugam, K. (1973). Textural Features for Image Classification.
644 *IEEE Trans. Syst. Man Cybern.* SMC-3, 610–621. doi: 10.1109/TSMC.1973.4309314.
- 645 Hastie, T., Tibshirani, R., and Friedman, J. (2005). The Elements of Statistical Learning : Data Mining ,
646 Inference and Prediction. *Math. Intell.* 27, 83–85. Available at:
647 <http://link.springer.com/article/10.1007/BF02985802?LI=true#>.
- 648 Jia, D., and Chen, P. (2020). Effect of Low-altitude UAV Image Resolution on Inversion of Winter
649 Wheat Nitrogen Concentration. *Nongye Jixie Xuebao/Transactions Chinese Soc. Agric. Mach.*
650 51, 164–169. doi: 10.6041/j.issn.1000-1298.2020.07.019.
- 651 Ju, X. T., Xing, G. X., Chen, X. P., Zhang, S. L., Zhang, L. J., Liu, X. J., et al. (2009). Reducing
652 environmental risk by improving N management in intensive Chinese agricultural systems. *Proc.*
653 *Natl. Acad. Sci. U. S. A.* 106, 3041–3046. doi: 10.1073/pnas.0813417106.
- 654 Kalacska, M., Lalonde, M., and Moore, T. R. (2015). Estimation of foliar chlorophyll and nitrogen
655 content in an ombrotrophic bog from hyperspectral data: Scaling from leaf to image. *Remote*
656 *Sens. Environ.* 169, 270–279. doi: 10.1016/j.rse.2015.08.012.
- 657 Kelsey, K. C., and Neff, J. C. (2014). Estimates of aboveground biomass from texture analysis of
658 landsat imagery. *Remote Sens.* 6, 6407–6422. doi: 10.3390/rs6076407.
- 659 Kitonyo, O. M., Sadras, V. O., Zhou, Y., and Denton, M. D. (2018). Nitrogen supply and sink demand
660 modulate the patterns of leaf senescence in maize. *F. Crop. Res.* 225, 92–103. doi:
661 10.1016/j.fcr.2018.05.015.
- 662 Klem, K., Záhora, J., Zemek, F., Trunda, P., Tůma, I., Novotná, K., et al. (2018). Interactive effects of
663 water deficit and nitrogen nutrition on winter wheat. Remote sensing methods for their detection.
664 *Agric. Water Manag.* 210, 171–184. doi: 10.1016/j.agwat.2018.08.004.
- 665 Kong, L., Sun, M., Xie, Y., Wang, F., and Zhao, Z. (2015). Photochemical and antioxidative responses

- 666 of the glume and flag leaf to seasonal senescence in wheat. *Front. Plant Sci.* 6, 1–10. doi:
667 10.3389/fpls.2015.00358.
- 668 Lemaire, G., Jeuffroy, M. H., and Gastal, F. (2008). Diagnosis tool for plant and crop N status in
669 vegetative stage. Theory and practices for crop N management. *Eur. J. Agron.* 28, 614–624. doi:
670 10.1016/j.eja.2008.01.005.
- 671 Li, D., Wang, X., Zheng, H., Zhou, K., Yao, X., Tian, Y., et al. (2018a). Estimation of area- and mass-
672 based leaf nitrogen contents of wheat and rice crops from water-removed spectra using
673 continuous wavelet analysis. *Plant Methods* 14, 1–20. doi: 10.1186/s13007-018-0344-1.
- 674 Li, F., Gnyp, M. L., Jia, L., Miao, Y., Yu, Z., Koppe, W., et al. (2008). Estimating N status of winter
675 wheat using a handheld spectrometer in the North China Plain. *F. Crop. Res.* 106, 77–85. doi:
676 10.1016/j.fcr.2007.11.001.
- 677 Li, F., Miao, Y., Feng, G., Yuan, F., Yue, S., Gao, X., et al. (2014). Improving estimation of summer
678 maize nitrogen status with red edge-based spectral vegetation indices. *F. Crop. Res.* 157, 111–
679 123. doi: 10.1016/j.fcr.2013.12.018.
- 680 Li, F., Miao, Y., Hennig, S. D., Gnyp, M. L., Chen, X., Jia, L., et al. (2010). Evaluating hyperspectral
681 vegetation indices for estimating nitrogen concentration of winter wheat at different growth
682 stages. *Precis. Agric.* 11, 335–357. doi: 10.1007/s11119-010-9165-6.
- 683 Li, H., Zhao, C., Yang, G., and Feng, H. (2015). Variations in crop variables within wheat canopies and
684 responses of canopy spectral characteristics and derived vegetation indices to different vertical
685 leaf layers and spikes. *Remote Sens. Environ.* 169, 358–374. doi: 10.1016/j.rse.2015.08.021.
- 686 Li, J., Shi, Y., Veeranampalayam-Sivakumar, A. N., and Schachtman, D. P. (2018b). Elucidating
687 sorghum biomass, nitrogen and chlorophyll contents with spectral and morphological traits
688 derived from unmanned aircraft system. *Front. Plant Sci.* 9, 1–12. doi: 10.3389/fpls.2018.01406.
- 689 Li, S., Ding, X., Kuang, Q., Ata-UI-Karim, S. T., Cheng, T., Liu, X., et al. (2018c). Potential of UAV-
690 based active sensing for monitoring rice leaf nitrogen status. *Front. Plant Sci.* 871, 1–14. doi:
691 10.3389/fpls.2018.01834.
- 692 Li, W., Zhou, X., Yu, K., Zhang, Z., Liu, Y., Hu, N., et al. (2021). Spectroscopic Estimation of N
693 Concentration in Wheat Organs for Assessing N Remobilization Under Different Irrigation
694 Regimes. *Front. Plant Sci.* 12, 1–11. doi: 10.3389/fpls.2021.657578.
- 695 Liang, T., Duan, B., Luo, X., Ma, Y., and Yuan, Z. (2021). Identification of High Nitrogen Use
696 Efficiency Phenotype in Rice (*Oryza sativa* L.) Through Entire Growth Duration by Unmanned
697 Aerial Vehicle Multispectral Imagery. 12. doi: 10.3389/fpls.2021.740414.
- 698 Liu, H., Zhu, H., and Wang, P. (2017). Quantitative modelling for leaf nitrogen content of winter wheat
699 using UAV-based hyperspectral data. *Int. J. Remote Sens.* 38, 2117–2134. doi:
700 10.1080/01431161.2016.1253899.
- 701 Liu, S., Li, L., Gao, W., Zhang, Y., Liu, Y., Wang, S., et al. (2018). Diagnosis of nitrogen status in
702 winter oilseed rape (*Brassica napus* L.) using in-situ hyperspectral data and unmanned aerial
703 vehicle (UAV) multispectral images. *Comput. Electron. Agric.* 151, 185–195. doi:
704 10.1016/j.compag.2018.05.026.
- 705 Lu, N., Wang, W., Zhang, Q., Li, D., Yao, X., Tian, Y., et al. (2019). Estimation of Nitrogen Nutrition
706 Status in Winter Wheat From Unmanned Aerial Vehicle Based Multi-Angular Multispectral
707 Imagery. *Front. Plant Sci.* 10. doi: 10.3389/fpls.2019.01601.
- 708 Maresma, Á., Ariza, M., Martínez, E., Lloveras, J., and Martínez-Casasnovas, J. A. (2016). Analysis of
709 vegetation indices to determine nitrogen application and yield prediction in maize (*zea mays* l.)

- 710 from a standard uav service. *Remote Sens.* 8. doi: 10.3390/rs8120973.
- 711 Maydup, M. L., Antonietta, M., Guiamet, J. J., and Tambussi, E. A. (2012). The contribution of green
712 parts of the ear to grain filling in old and modern cultivars of bread wheat (*Triticum aestivum* L.):
713 Evidence for genetic gains over the past century. *F. Crop. Res.* 134, 208–215. doi:
714 10.1016/j.fcr.2012.06.008.
- 715 Mevik, B. H., and Wehrens, R. (2007). The pls package: Principal component and partial least squares
716 regression in R. *J. Stat. Softw.* 18, 1–23. doi: 10.18637/jss.v018.i02.
- 717 Murray, H., Lucieer, A., and Williams, R. (2010). Texture-based classification of sub-Antarctic
718 vegetation communities on Heard Island. *Int. J. Appl. Earth Obs. Geoinf.* 12, 138–149. doi:
719 10.1016/j.jag.2010.01.006.
- 720 Nigon, T. J., Mulla, D. J., Rosen, C. J., Cohen, Y., Alchanatis, V., Knight, J., et al. (2015).
721 Hyperspectral aerial imagery for detecting nitrogen stress in two potato cultivars. *Comput.*
722 *Electron. Agric.* 112, 36–46. doi: 10.1016/j.compag.2014.12.018.
- 723 Nigon, T. J., Yang, C., Paiao, G. D., Mulla, D. J., Knight, J. F., and Fernández, F. G. (2020). Prediction
724 of early season nitrogen uptake in maize using high-resolution aerial hyperspectral imagery.
725 *Remote Sens.* 12. doi: 10.3390/RS12081234.
- 726 Ohyama Takuji (2010). Nitrogen as a major essential element of plants. *Nitrogen Assim. plants* 37, 2–
727 17.
- 728 Onojeghuo, A. O., Blackburn, G. A., Huang, J., Kindred, D., and Huang, W. (2018). Applications of
729 satellite ‘hyper-sensing’ in Chinese agriculture: Challenges and opportunities. *Int. J. Appl. Earth*
730 *Obs. Geoinf.* 64, 62–86. doi: 10.1016/j.jag.2017.09.005.
- 731 Sanchez-Bragado, R., Elazab, A., Zhou, B., Serret, M. D., Bort, J., Nieto-Taladriz, M. T., et al. (2014).
732 Contribution of the ear and the flag leaf to grain filling in durum wheat inferred from the carbon
733 isotope signature: Genotypic and growing conditions effects. *J. Integr. Plant Biol.* 56, 444–454.
734 doi: 10.1111/jipb.12106.
- 735 Sanchez-Bragado, R., Molero, G., Reynolds, M. P., and Araus, J. L. (2016). Photosynthetic
736 contribution of the ear to grain filling in wheat: A comparison of different methodologies for
737 evaluation. *J. Exp. Bot.* 67, 2787–2798. doi: 10.1093/jxb/erw116.
- 738 Schroder, J. L., Zhang, H., Girma, K., Raun, W. R., Penn, C. J., and Payton, M. E. (2011). Soil
739 Acidification from Long-Term Use of Nitrogen Fertilizers on Winter Wheat. *Soil Sci. Soc. Am. J.*
740 75, 957–964. doi: 10.2136/sssaj2010.0187.
- 741 Sinclair, T. R., Rufty, T. W., and Lewis, R. S. (2019). Increasing Photosynthesis: Unlikely Solution For
742 World Food Problem. *Trends Plant Sci.* 24, 1032–1039. doi: 10.1016/j.tplants.2019.07.008.
- 743 Song, X., Feng, W., He, L., Xu, D., Zhang, H. Y., Li, X., et al. (2016). Examining view angle effects
744 on leaf N estimation in wheat using field reflectance spectroscopy. *ISPRS J. Photogramm.*
745 *Remote Sens.* 122, 57–67. doi: 10.1016/j.isprsjprs.2016.10.002.
- 746 Stroppiana, D., Boschetti, M., Brivio, P. A., and Bocchi, S. (2009). Plant nitrogen concentration in
747 paddy rice from field canopy hyperspectral radiometry. *F. Crop. Res.* 111, 119–129. doi:
748 10.1016/j.fcr.2008.11.004.
- 749 T., T., I., A., and T., O. (1986). The diagnosis of nitrogen nutrition of rice plants (Sasanishiki) using
750 chlorophyll-meter. *Japanese J. Soil Sci. Plant Nutr.* v. 57.
- 751 Tian, Y. C., Yao, X., Yang, J., Cao, W. X., Hannaway, D. B., and Zhu, Y. (2011). Assessing newly
752 developed and published vegetation indices for estimating rice leaf nitrogen concentration with
753 ground- and space-based hyperspectral reflectance. *F. Crop. Res.* 120, 299–310. doi:

- 754 10.1016/j.fcr.2010.11.002.
- 755 Tilly, N., and Bareth, G. (2019). Estimating nitrogen from structural crop traits at field scale—a novel
756 approach versus spectral vegetation indices. *Remote Sens.* 11. doi: 10.3390/rs11172066.
- 757 Vergara-Díaz, O., Vatter, T., Kefauver, S. C., Obata, T., Fernie, A. R., and Araus, J. L. (2020).
758 Assessing durum wheat ear and leaf metabolomes in the field through hyperspectral data. *Plant J.*
759 102, 615–630. doi: 10.1111/tpj.14636.
- 760 Verrelst, J., Camps-Valls, G., Muñoz-Marí, J., Rivera, J. P., Veroustraete, F., Clevers, J. G. P. W., et al.
761 (2015). Optical remote sensing and the retrieval of terrestrial vegetation bio-geophysical
762 properties - A review. *ISPRS J. Photogramm. Remote Sens.* 108, 273–290. doi:
763 10.1016/j.isprsjprs.2015.05.005.
- 764 Vicente, R., Vergara-Díaz, O., Medina, S., Chairi, F., Kefauver, S. C., Bort, J., et al. (2018). Durum
765 wheat ears perform better than the flag leaves under water stress: Gene expression and
766 physiological evidence. *Environ. Exp. Bot.* 153, 271–285. doi: 10.1016/j.envexpbot.2018.06.004.
- 767 Wan, S., and Chang, S. H. (2019). Crop classification with WorldView-2 imagery using Support
768 Vector Machine comparing texture analysis approaches and grey relational analysis in Jianan
769 Plain, Taiwan. *Int. J. Remote Sens.* 40, 8076–8092. doi: 10.1080/01431161.2018.1539275.
- 770 Wang, F., Yang, M., Ma, L., Zhang, T., Qin, W., Li, W., et al. (2022a). Estimation of Aboveground
771 Biomass of Winter Wheat Based on Consumer-Grade Multi-Spectral UAV. 14, 1251. Available
772 at: <https://doi.org/10.3390/rs14051251>.
- 773 Wang, L., Chang, Q., Li, F., Yan, L., Huang, Y., Wang, Q., et al. (2019). Effects of growth stage
774 development on paddy rice leaf area index prediction models. *Remote Sens.* 11, 1–18. doi:
775 10.3390/rs11030361.
- 776 Wang, W., Yao, X., Yao, X. F., Tian, Y. C., Liu, X. J., Ni, J., et al. (2012). Estimating leaf nitrogen
777 concentration with three-band vegetation indices in rice and wheat. *F. Crop. Res.* 129, 90–98.
778 doi: 10.1016/j.fcr.2012.01.014.
- 779 Wang, Y. P., Chang, Y. C., and Shen, Y. (2022b). Estimation of nitrogen status of paddy rice at
780 vegetative phase using unmanned aerial vehicle based multispectral imagery. *Precis. Agric.* 23.
781 doi: 10.1007/s11119-021-09823-w.
- 782 Wang, Z., Skidmore, A. K., Darvishzadeh, R., Heiden, U., Heurich, M., and Wang, T. (2015). Leaf
783 Nitrogen Content Indirectly Estimated by Leaf Traits Derived from the PROSPECT Model.
784 *IEEE J. Sel. Top. Appl. Earth Obs. Remote Sens.* 8, 3172–3182. doi:
785 10.1109/JSTARS.2015.2422734.
- 786 Wang, Z., Zhang, W., Beebout, S. S., Zhang, H., Liu, L., Yang, J., et al. (2016). Grain yield, water and
787 nitrogen use efficiencies of rice as influenced by irrigation regimes and their interaction with
788 nitrogen rates. *F. Crop. Res.* 193, 54–69. doi: 10.1016/j.fcr.2016.03.006.
- 789 Wen, P., Shi, Z., Li, A., Ning, F., Zhang, Y., Wang, R., et al. (2021). Estimation of the vertically
790 integrated leaf nitrogen content in maize using canopy hyperspectral red edge parameters. *Precis.*
791 *Agric.* 22, 984–1005. doi: 10.1007/s11119-020-09769-5.
- 792 Wold, S., Sjöström, M., and Eriksson, L. (2001). PLS-regression: A basic tool of chemometrics.
793 *Chemom. Intell. Lab. Syst.* 58, 109–130. doi: 10.1016/S0169-7439(01)00155-1.
- 794 Xue, L., Cao, W., Luo, W., Dai, T., and Zhu, Y. (2004). Monitoring Leaf Nitrogen Status in Rice with
795 Canopy Spectral Reflectance. *Agron. J.* 96, 135–142. doi: 10.2134/agronj2004.0135.
- 796 Yang, G., Zhao, C., Pu, R., Feng, H., Li, Z., Li, H., et al. (2015). Leaf nitrogen spectral reflectance
797 model of winter wheat (*Triticum aestivum*) based on PROSPECT: simulation and inversion. *J.*

- 798 *Appl. Remote Sens.* 9, 095976. doi: 10.1117/1.jrs.9.095976.
- 799 Yang, K., Gong, Y., Fang, S., Duan, B., Yuan, N., Peng, Y., et al. (2021). Combining spectral and
800 texture features of uav images for the remote estimation of rice lai throughout the entire growing
801 season. *Remote Sens.* 13. doi: 10.3390/rs13153001.
- 802 Yang, M., Hassan, M. A., Xu, K., Zheng, C., Rasheed, A., Zhang, Y., et al. (2020). Assessment of
803 Water and Nitrogen Use Efficiencies Through UAV-Based Multispectral Phenotyping in Winter
804 Wheat. *Front. Plant Sci.* 11, 1–16. doi: 10.3389/fpls.2020.00927.
- 805 Yao, X., Huang, Y., Shang, G., Zhou, C., Cheng, T., Tian, Y., et al. (2015). Evaluation of six
806 algorithms to monitor wheat leaf nitrogen concentration. *Remote Sens.* 7, 14939–14966. doi:
807 10.3390/rs71114939.
- 808 Yu, K., Lenz-Wiedemann, V., Chen, X., and Bareth, G. (2014). Estimating leaf chlorophyll of barley at
809 different growth stages using spectral indices to reduce soil background and canopy structure
810 effects. *ISPRS J. Photogramm. Remote Sens.* 97, 58–77. doi: 10.1016/j.isprsjprs.2014.08.005.
- 811 Yu, K., Li, F., Gnyp, M. L., Miao, Y., Bareth, G., and Chen, X. (2013). Remotely detecting canopy
812 nitrogen concentration and uptake of paddy rice in the Northeast China Plain. *ISPRS J.*
813 *Photogramm. Remote Sens.* 78, 102–115. doi: 10.1016/j.isprsjprs.2013.01.008.
- 814 Yuan, Z., Ata-Ul-Karim, S. T., Cao, Q., Lu, Z., Cao, W., Zhu, Y., et al. (2016). Indicators for
815 diagnosing nitrogen status of rice based on chlorophyll meter readings. *F. Crop. Res.* 185, 12–20.
816 doi: 10.1016/j.fcr.2015.10.003.
- 817 Yue, J., Yang, G., Tian, Q., Feng, H., Xu, K., and Zhou, C. (2019). Estimate of winter-wheat
818 aboveground biomass based on UAV ultrahigh-ground-resolution image textures and vegetation
819 indices. *ISPRS J. Photogramm. Remote Sens.* 150, 226–244. doi:
820 10.1016/j.isprsjprs.2019.02.022.
- 821 Zhang, H. Y., Ren, X. X., Zhou, Y., Wu, Y. P., He, L., Heng, Y. R., et al. (2018). Remotely assessing
822 photosynthetic nitrogen use efficiency with in situ hyperspectral remote sensing in winter wheat.
823 *Eur. J. Agron.* 101, 90–100. doi: 10.1016/j.eja.2018.08.010.
- 824 Zheng, H., Cheng, T., Zhou, M., Li, D., Yao, X., Tian, Y., et al. (2019). Improved estimation of rice
825 aboveground biomass combining textural and spectral analysis of UAV imagery. *Precis. Agric.*
826 20, 611–629. doi: 10.1007/s11119-018-9600-7.
- 827 Zheng, H., Li, W., Jiang, J., Liu, Y., Cheng, T., Tian, Y., et al. (2018). A comparative assessment of
828 different modeling algorithms for estimating leaf nitrogen content in winter wheat using
829 multispectral images from an unmanned aerial vehicle. *Remote Sens.* 10. doi:
830 10.3390/rs10122026.
- 831 Zheng, H., Ma, J., Zhou, M., Li, D., Yao, X., Cao, W., et al. (2020). Enhancing the nitrogen signals of
832 rice canopies across critical growth stages through the integration of textural and spectral
833 information from unmanned aerial vehicle (UAV) multispectral imagery. *Remote Sens.* 12. doi:
834 10.3390/rs12060957.
- 835 Zhu, W., Rezaei, E. E., Nouri, H., Sun, Z., Li, J., Yu, D., et al. (2022). UAV-based indicators of crop
836 growth are robust for distinct water and nutrient management but vary between crop development
837 phases. *F. Crop. Res.* 284, 108582. doi: 10.1016/j.fcr.2022.108582.
- 838
- 839